HHS Public Access

Author manuscript

Anal Chem. Author manuscript; available in PMC 2018 January 03.

Published in final edited form as:

Anal Chem. 2017 January 03; 89(1): 42–56. doi:10.1021/acs.analchem.6b04672.

Recent Advances in the Development of Highly Luminescent Semiconducting Polymer Dots and Nanoparticles for Biological Imaging and Medicine

Jiangbo Yu, **Yu Rong**, **Chun-Ting Kuo**, **Xing-Hua Zhou**, and **Daniel T. Chiu***

Department of Chemistry, University of Washington, Seattle, Washington 98195, United States

Semiconducting polymer dots (Pdots) have been developed as a brightly emissive nanoprobe for biological analysis and imaging, as well as for diagnosis and drug delivery (therapy). Pdots are well-suited for these different applications because they have exceptional photophysical properties, including large extinction coefficients, high single-particle brightness, and excellent photostability. Pdots also possess good biocompatibility, tunable optical properties and surface properties and colloidal dimensions. Several reviews and perspectives have described conjugated polymer nanoparticles (CPN) in the past decade,[1–19] but we consider only some of these CPNs to be Pdots. As described in our previous review,[11] Pdots connote both small particle size and high brightness. Therefore, we view Pdots to be a subset of CPNs.[11] To be consistent with the notion of a small "dot", Pdots should be less than 20–30 nm in diameter, preferably in the 5–20 nm range. As the weight or volume fraction of semiconducting polymers largely determines the fluorescence brightness, Pdots should comprise more than 50% semiconducting polymer, either in weight or in volume, preferably with greater than 80% semiconducting polymer. Finally, Pdots should have a hydrophobic polymer interior.[11] If the reported semiconducting polymer nanoprobes do not satisfy the above three criteria, we will refer to them more generally as semiconducting or conjugated polymer nanoparticles (CPNs).

Our previous review presented our definition of Pdots, described their preparation methods, and discussed their properties and performances, including particle size/morphology, photophysical properties, colloidal/chemical properties, and toxicity. We also reviewed the functionalization and bioconjugation of Pdots, the biological applications of Pdots including cellular labeling through endocytosis, immunofluorescence labeling, biorthogonal labeling by click chemistry, the in vivo imaging, and single-particle tracking using Pdots, and sensors and drug/gene delivery systems based on Pdots. Given the utility and potential applications of CPNs in general, and Pdots in particular, it is not surprising that more than 100 peer-reviewed articles have been published in this area since 2013, the year of our last review. Here, we will focus primarily on advances made in the past few years. However, this article is not meant to be a comprehensive review but rather a highlight of recent advances.

*Corresponding Author, chiu@uw.edu.

The authors declare no competing financial interest.

We would also like to refer readers to several other recent reviews and perspectives that discuss CPNs or Pdots in different applications. For example, Pdots and CPNs have been discussed and compared to other nanoprobes, such as dye-loaded nanobeads,[13,17,18] semiconductor quantum dots (Qdots),[13,16] and carbon dots.[13,18] We recently performed a systematic comparative study on the cytotoxicity of Pdots and Qdots, both at the gross cell level (e.g., cell viability, proliferation, and necrosis) and at a molecular level (e.g., redox stress).[20] These recent reviews, perspectives, and research articles suggest that Pdots are preferable for many biomedical applications. In this Review, we mainly will highlight recent advances of luminescent Pdots (including fluorescence, phosphorescence, and electro- and chemiluminescence) or CPNs that are comprised of more than 50% semiconducting polymer. The list of topics include narrow emissive Pdots for multiplexing,[21–26] near-infrared (NIR) emissive Pdots and CPNs,[23,26–35] long luminescence lifetime emissive Pdots and CPNs,[22,24,32] single-chain and monovalent Pdots,[36,37] photoswitchable Pdots and CPNs,[38–43] electro-/chemiluminescent Pdots and CPNs,[44–54] CPNs with aggregation-induced emission (AIE),[52,55–60] luminescent Pdots and CPNs for dual modality imaging,[61–65] and Pdots and CPNs developed for biosensing[66–81] and photodynamic cancer therapy.[82–86]

NARROW EMISSIVE Pdots FOR MULTIPLEXING

The first-generation Pdots exhibited broad emission spectra.[11] The broad emission spectra limited the biomedical applications of these Pdots, especially those that require multiplexing, such as flow cytometry and cell sorting, in vitro/in vivo imaging, Western blot analysis, and immunofluorescence or nucleic acid analysis. To address this limitation of the first-generation Pdots, we developed a series of Pdots based on boron dipyrromethene (BODIPY), in which BODIPY monomers were covalently incorporated into the semiconducting polymer chain and used as an emitter.[21,23,25] BODIPY is known as an excellent fluorescent probe, with a high molar extinction coefficient, high fluorescence quantum yield (QY), sharp emission spectra, excellent chemical and photophysical stabilities, and low toxicity.[87] The covalent incorporation of BODIPY into the semiconducting polymer chain enabled us to design and create a comprehensive series of Pdots with emission spanning the visible to NIR region.[21,23,25]

These BODIPY Pdots had narrow emission width (full-width-at-half-maximum (fwhm) of ~40–55 nm), which was 1.5–2 times narrower than those of the first-generation Pdots (Figure 1). Because we directly polymerized monomers with the carboxylate groups into the polymer backbone, we could conveniently carry out bioconjugation of the Pdots with biological molecules, such as streptavidin (SA).[21] As an example, one green-colored BODIPY520 Pdot with a comparable size with Qdot525 was studied using single-particle imaging (Figure 1b) and flow cytometry (Figure 1c) where the brightness of cells labeled with BODIPY520 Pdot and Qdot525 was compared using identical experimental conditions. Both the single-particle imaging and flow-cytometry measurements concluded that, under 405 nm laser excitation, BODIPY520 Pdots were brighter than Qdot525 by about an order of magnitude.[21] Confocal fluorescence microscopy experiments also showed the series of BODIPY Pdot probes that stained cells specifically; three differently colored BODIPY Pdot-labeled cells could be distinguished easily in their respective fluorescence channels (Figure

1a). Using a polymer cross-linking approach we reported previously,[88] we also developed a yellow BODIPY565 Pdot, which exhibited a narrow fwhm of only 37 nm and a small Pdot size of 12 nm in diameter.[25] Similar to our other BODIPY-based Pdots,[21] this yellow BODIPY565 Pdot also possessed high brightness and high photostability when compared with the commercial Qdot565.

Furthermore, by tuning the structure of the BODIPY-based emitter, we also developed BODIPY Pdots with NIR emission,[23] which we will describe together with squaraine-based Pdots,[26] in the next section on NIR emission. In addition to all organic Pdots that offer narrow emission, lanthanide (Ln) complexes are known to have extremely narrow emission.[89] To take advantage of the ultranarrow emission of Ln complexes, we developed a bright Ln-Pdot by incorporating europium complexes (Eu15F) into the semiconducting polymer poly(9-vinylcarbazole) (PVK).[22,24] Efficient energy transfer between the donor PVK and the acceptor Eu15F led to very bright and ultranarrow red emission with a fwhm of only 8 nm. We will describe these Ln-Pdots in more detail in a later section on Pdots with long luminescence lifetime.

NIR-EMISSIVE Pdots AND CPNs

NIR-emissive fluorescence probes are highly desirable for imaging. They are especially needed for in vivo applications because the NIR region offers maximal penetration into biological tissues, good spectral separation from autofluorescence, and less scattering in turbid media. One challenging issue encountered in the development of most of the NIR emitters is self-quenching because, at the molecular level, NIR emitters have extended π-conjugations that tend to lower their solubility in aqueous solution and increase their tendency to aggregate and self-quench. This issue is partly overcome with Pdots, because the Pdot interior is hydrophobic and thus serves as a good environment to host NIR chromophores.

Previously, we reported Pdots doped with NIR dyes.[90] However, potential issues of dye leakage from Pdots, especially in long-term biological applications, prompted us to further develop NIR-emissive Pdots. This effort resulted in the design of NIR BODIPY-based[23] and squaraine-based semiconducting polymers[26] with the NIR emitting unit forming part of the backbone of the semiconducting polymer. As shown in Figure 2, after careful design and polymerization of the donors, acceptors, and energy transfer units into the backbone of the semiconducting polymer, four polymers (P1, P2, P3, and P4 containing donors and acceptors (emitter); see Figure 2a top inset) were obtained for preparing NIR Pdots. Using cascade Förster resonance energy transfer (FRET) and careful tuning of the ratios of donors, acceptors, and energy transfer units, we made highly luminescent NIR-emissive Pdots: **3-NIR** Pdots (prepared from blending polymers of P1, P2, and P4) with emission peak at 720 nm and **4-NIR** Pdots (prepared from blending polymers of P1-P4) with emission peak at 710 nm. The Pdots had narrow fluorescence band (fwhm ~40 nm) and large Stoke shifts (i.e., absorption–emission separation) (Figure 2b). From the absorption/fluorescence spectra and time-resolved fluorescence decay (Figure 2c) measured using time-correlated single-photon counting (TCSPC) techniques, we found there were efficient FRET processes occurring within the Pdots (final QY > 30%). Single-particle fluorescence measurements and flow

cytometry analysis of Pdot-labeled cells showed these NIR emitting Pdots were several times brighter than Qdot705 (Figure 2d); confocal fluorescence images of cells positively labeled with NIR-emissive Pdot probes showed high brightness with minimal cell autofluorescence (Figure 2e).

This work illustrated several benefits of Pdots: (1) excellent light harvesting capability of the semiconducting polymer, resulting in high brightness; (2) efficient cascade FRET in Pdots, offering tunable emission with large Stoke shifts; (3) hydrophobic Pdot interior that serves as a good host for NIR emitters through polymerization, overcoming solubility issues in aqueous solution. This work points to a general strategy for the preparation of different NIR-emitting Pdots for various biological applications. In addition to BODIPY-Pdots with NIR emission, we also designed squaraine-based Pdots with NIR emission.[26] When excited at 405 nm, the squaraine-based Pdots (PFS) showed NIR emission peaks at 693 and 710 nm with QYs of 30% and 17%, respectively. Both BODIPY Pdots and squaraine Pdots showed a large Stokes shift (>300 nm), but the molecular mechanism responsible for efficient energy transfer and this large Stoke shift may be different in each type of Pdot. For BODIPY Pdots, we relied on cascade FRET, but in squaraine Pdots, we found efficient energy transfer despite minimal spectral overlap between donor and acceptor, a requirement for FRET. Instead of FRET, we hypothesized energy transfer occurred via efficient exciton diffusion along the polymer chain containing mostly donors, followed by through-bond energy transfer between the donor (fluorene) and the acceptor (squaraine). We believe this mechanism will inspire us and others to develop more NIR-emissive Pdots with large Stokes shift, high quantum yield, and narrow emission bandwidth, even in the absence of significant spectral overlap between the energy donor and the acceptor.

Besides the above NIR-emissive Pdots, Rao and co-workers used silicon 2,3-naphthalocyanine bis(trihexylsilyloxide) (NIR775) dyes doped into poly[2-methoxy-5-(2-ethylhexyloxy)-1,4-phenylenevinylene] (MEH-PPV) semiconducting polymers to prepare NIR-emissive Pdots or CPNs.[27,32] Rao and co-workers observed efficient FRET, which was similar to our observation with NIR775 doped into PFBT semiconducting polymer.[90] Rather than relying on optical excitation, which has issues with penetration depth, Rao and co-workers innovatively employed an energy transfer scheme that integrated both bioluminescence resonance energy transfer (BRET) and FRET, which enabled them to carry out in vivo lymph-node mapping and cancer imaging without using external light excitation and with excellent tumor-to-background ratio (>100). Another highly interesting observation they reported is that these NIR775/MEH-PPV CPNs exhibit persistent luminescence (long luminescence lifetime), which they exploited for in vivo imaging. This result will be discussed in greater detail in the next section about long luminescence lifetime Pdots.

A number of other interesting studies have been reported by several research groups. [27,28,30–35] For example, Chan and co-workers described NIR-emissive Pdots using semiconducting polymers with red-shifted emitters obtained by modification of the emitters' structures.[28,30,31,34] Xiong et al. developed similar MEH-PPV/NIR775-based CPNs as Rao's group that could be used for tumor cell imaging in vitro and in vivo. [33,35]

LONG LUMINESCENCE LIFETIME EMISSIVE Pdots AND CPNs

Long luminescence lifetime (or long excited-state lifetime) generally arises from the decay of the triplet states of emitters. The lifetime usually is on the order of microseconds (μs) to milliseconds (ms). It is well-known many lanthanide compounds have long luminescence lifetime from μs to ms.[91] Other materials can exhibit even longer luminescence lifetimes, up to minutes and even hours; these very long luminescence lifetimes usually are referred to as "persistent luminescence", a phenomenon often found in solid materials doped with rare earth ions.[92] In contrast, the lifetime of fluorescence and autofluorescence is typically very short, on the order of nanoseconds (ns). The use of luminescent probes with long lifetimes for imaging thus has the advantage that it is easy to separate the luminescence signal from the autofluorescence background, resulting in significantly improved signal-to-noise (S/N) ratio. With this advantage in mind, we designed a new type of Pdot by incorporating Ln complexes into the host semiconducting polymer. The specific Ln complex we used was an Eu-complex (emitter) and the semiconducting polymer was the PVK polymer (donor). We found PVK not only functioned as a host matrix to disperse Eu-complex molecules, which reduced self-quenching among Eu-complexes, but also acted as an efficient light harvester and energy donor to sensitize the emission of Eu-complex through FRET. The Eu-complex/PVK Pdots possessed ultranarrow red fluorescence emission bandwidth of 8 nm and high emission brightness with QY > 30%. The Eu-complex/PVK Pdots showed a long luminescence lifetime of 509 μs. This long lifetime enabled us to use time-gated fluorescence microscopy to easily differentiate the small (<20 nm) Eu-complex/PVK Pdots in a background of large and bright fluorescent beads (R300; 300 nm diameter beads) that emit in the same wavelength range (emission peak at 612 nm) but with a fluorescence lifetime of 3.6 ns (Figure 3a–d). Cells labeled with Eu15F/PVK Pdots also were imaged with excellent S/N ratio (Figure 3e–i); from the figures, it is evident the background fluorescence in the time-gated cell images (Figure 3g,i) was much lower than that in the ungated ones (Figure 3e,h), because cellular autofluorescence was on the order of ns,[93] and thus efficiently filtered out. The S/N ratio was improved from 85 in the ungated image to 232 in the time-gated image.

As previously mentioned, Rao and co-workers found that NIR775/MEH-PPV CPNs have NIR persistent luminescence, lasting for 1 h upon a single excitation exposure to white light.[32] They ascribed this phenomenon to the host semiconducting polymer MEH-PPV in CPNs: Upon light excitation, the absorbed energy was stored in the MEH-PPV double bonds, after which the trapped excitation energy may re-emit as light through stimulated release by application of activation energy. In the presence of an acceptor (NIR775 dye) that was close to the semiconducting polymer (MEH-PPV), this released energy could be transferred to the acceptor to result in NIR persistent luminescence. Rao and co-workers have successfully applied this phenomenon for in vivo imaging.

SINGLE-CHAIN OR MONOVALENT Pdots

For many biological applications, especially those that involve the labeling of cell-surface receptors, Pdots with diameters less than 20 to 30 nm seem to work well.[94] From our previous studies, we found Pdots with diameters <10 nm labeled subcellular features (e.g.,

microtubules) much more efficiently than larger Pdots (>15–20 nm);[88,95] microtubules labeled with larger Pdots appeared more spotty in confocal fluorescence images.[96]

Additionally, small Pdots are less prone than large Pdots to alter the diffusional or biological activity of the molecules that they label. Small Pdots also can access crowded and size-restricted cellular/subcellular space, such as synapses, more efficiently. Finally, a small Pdot that consists of a single polymer chain can cause it to adopt an ultrasmall compact conformation, resulting in decreased nonspecific binding because of the Pdot's reduced surface area. Single-chain Pdots (*s*Pdots) will also result in Pdots with a highly monodisperse size distribution. We believe *s*Pdots having a diameter of <10 nm will offer better performance than conventional Pdots. Many applications, such as super-resolution imaging or dynamic analysis of subcellular structures, will benefit from this new generation of *s*Pdots.

In addition to *s*Pdots, monovalent Pdots (*m*Pdots) with a single functional group or conjugated biomolecule also are highly desired for many biological applications. *m*Pdots can be particularly useful for those applications that are sensitive to protein–nanoparticle clustering and aggregation. However, *s*Pdots or *m*Pdots cannot be prepared using conventional Pdot preparation methods, such as nanoprecipitation or microemulsion, which usually cause the coprecipitation of multiple polymer chains into one single Pdot. To overcome this limitation of conventional Pdot preparation methods, we explored a new approach to form *s*Pdots or *m*Pdots (Figure 4).[36,37] To implement this strategy, we synthesized a green emitting semiconducting polymer (alkyne terminated linear poly(*p*-phenylenevinylene) containing two pendent pentaphenylene groups (PPV–PPA)), from which we created *m*Pdots (see Figure 4 for details). Besides PPV–PPA *m*Pdots, we also prepared sPdots from the alkyne-functionalized semiconducting polymer poly[(9,9-dioctylfluorenyl-2,7-diyl)-*co*-(1,4-benzo-{2,10,3}-thiadazole)] (PFBTA) and poly[(9,9-dioctylfluorenyl-2,7-diyl)-*co*-(9,9-dipropylcarboxylfluorenyl-2,7-diyl)] (PFOA). To validate these Pdots were indeed *s*Pdots or *m*Pdots, we characterized them using transmission electron microscopy (TEM), atomic force microscopy (AFM), and dynamic light scattering (DLS). These measurements confirmed these Pdots were monovalent, and their small particle size of ~5 nm is consistent with the molecular weight of a single polymer chain. To further confirm *s*Pdots indeed contained a single polymer chain, we also designed a FRET assay that could discern the presence of more than one polymer chain present in a Pdot. This assay confirmed that *s*Pdots contained a single polymer chain. Finally, we found the exact particle size varied as a function of the molecular weight of the polymer chain. Although we successfully demonstrated the formation of *s*Pdots and *m*Pdots, we are currently working to improve the yield of the preparation procedure. Once *s*Pdots and *m*Pdots can be produced easily with high yield, we anticipate they will offer improved performance over conventional Pdots for many biomedical applications.

PHOTOSWITCHABLE Pdots AND CPNs

The ability to turn Pdots "on" and "off" with light is a highly useful capability. For example, Pdots that can be turned "on" or "off" (i.e., photoswitched) in a binary fashion will enable super-resolution imaging. However, at present, all photoswitchable Pdots[38,41,43] and

CPNs[39,40,42] reported so far cannot be turned "on" and "off" in a single-step stochastic binary fashion. Nevertheless, the reported analog photoswitchable Pdots can benefit other biological applications. As an example, we recently described an approach to optically sort cells that used photoswitchable Pdots as cell paint.[41]

Fluorescence-activated cell sorting (FACS) is a powerful and widely used method to sort individual cells of interest based on biomarker expression. FACS, however, requires a suspension of cells. As a result, FACS cannot be used to sort cells based on the cell's appearance on a culture plate or its spatial location in a tissue. To address this limitation of FACS, we used photoswitchable Pdots as an optical "painting" tool under a microscope, which enabled the optical marking of individual cells based on their spatial and morphological features. Once marked, the cells could be dissociated from the culture plate or tissue for recovery using FACS.

As depicted in Figure 5a, we first designed and synthesized a new type of photoswitchable Pdot, which could be switched between the bright (ON) and dark (OFF) states reversibly. Figure 5b shows these photoswitchable Pdots had a 150-fold contrast ratio between the OFF and ON state; we used ultraviolet light for switching OFF the Pdots and red light for switching ON the Pdots. We then labeled cells with photoswitchable Pdot-streptavidin via biotinylated primary antibody against cell-surface receptors (Figure 5a). With a focused 633 nm laser beam, we could select and "paint" individual adherent cells under a microscope and even parts of a single cell. Once painted, we could recover these cells with 90% recovery efficiency and near 100% purity. We were able to carry out additional analysis of the recovered cells, including Sanger sequencing and mRNA extraction. This method has also been applied to paint individual cells in a murine pancreatic tumor tissue slice (Figure 5c – j). With automation, this method has the potential to achieve high throughput for the optical marking and sorting of individual adherent cells.

ELECTROCHEMILUMINESCENT AND CHEMILUMINESCENT Pdots AND CPNs

Barbara and co-workers first reported the electrochemiluminescence (ECL) studies of PFBT CPNs[45] using single-molecule spectroelectrochemistry (SMS-EC).[44,45] Their typical working process was based on rapid electrochemical (EC) reaction of PFBT CPNs immobilized at an ITO working electrode in an EC cell. The EC cell was filled with acetonitrile solution containing $LiClO_4$ as supporting electrolyte and a coreactant (tri-*n*-propylamine, TPrAH). Under different cell currents and applied potentials, TPrAH was oxidized; the resulting PFBT·+ hole was transported by hole-hopping along the surface of CPN. The reaction between the PFBT·+ with the radical TPrA· produced the excited state in the polymer chain of PFBT CPN, from which ECL was detected. Barbara and co-workers' initial motivation was to use SMS-EC to study the energetics and dynamics of deep traps in organic materials, which are often used in solar cells and organic LEDs at the nanoscale. However, this method may be developed into a sensitive analytical method for biological applications because of the high sensitivity, low background, high spatial, and high temporal resolution of ECL.

Recently, several research groups have reported ECL in other Pdots[50] and CPNs[47–49,53] composed of different semiconducting polymers. They also applied ECL Pdots or CPNs as sensors. For example, Chen and co-workers have described ECL of PFO CPNs;[48,49] Chi and co-workers have studied two kinds of CPNs prepared from the semiconducting polymers MEH-PPV and poly[(9,9-di(2-ethylhexyl)-9*H*–fluorene-2,7-vi-nylene)-*co*-(1-methoxy-4-(2-ethylhe-xyloxy)-2,5-phenylenevinylene)] (PPV);[47,53] Cheng and co-workers have synthesized a silole-containing polymer (SCP) and prepared Pdots to explore their ECL properties.[50]

In Chi and co-workers' studies of MEH-PPV CPNs, they capped them with Triton X-100 surfactant and studied the MEH-PPV CPNs' ECL in aqueous solution.[47] They found these CPNs had excellent and multichannel ECL properties at the glassy carbon/water interface, such as removing ECL activity in the absence of coreactants and producing bright anodic and cathodic ECL emissions at 590 nm in the presence of TPrA and perxoydisulfate ($S_2O_8^{2-}$), respectively. They also found that the surfactant Triton X-100 played an important role in the ECL of CPNs, where it rendered the surface of CPNs more hydrophilic (soluble) in water so that the ECL reactions proceeded more efficiently. They discussed the mechanism of ECL in their studies and proposed that the versatile ECL properties of the hydrophilic CPNs, combined with their low cytotoxicity, good biocompatibility, and easy bioconjugation, may lead to promising applications of this new type of ECL nanomaterial in biosensing and biological imaging, as well as new types of light-emitting devices. Using the same strategy, they also studied ECL of PPV CPNs.[53]

In Chen and co-workers' studies, they first investigated the anodic ECL behavior of PFO CPNs with $Na_2C_2O_4$ as the coreactant for sensing melamine, which efficiently quenched ECL.[48] Then, they prepared nanocomposite C_{60}-PAMAM-PFO, which was formed via electrostatic interaction between the negative charged PFO CPNs and the positively charged C_{60}-PAMAM (polyamidoamine) nanoparticles.[49] With this C_{60}-PAMAM-PFO nanocomposite in the presence of oxidoreductase, they found the ECL behavior of PFO CPNs was enhanced when H_2O_2 was used as a coreactant. As a result, this ECL nanocomposite material was used as a biosensor to detect H_2O_2 using Chox as the model enzyme. Furthermore, Chen and co-workers proposed that this PFO–H_2O_2 system may be used to replace the luminol–H_2O_2 system for detecting oxidoreductase-based substrates, such as choline, lactate, glucose, and acetylcholine.

In another work, Cheng and co-workers prepared a silole-containing Pdot (SCP Pdot) (Figure 6a) and studied its ECL-related properties, such as measuring its cyclic voltammograms and ECL intensity-potential curves under different conditions. These experiments reported strong anodic ECL emission in the presence of TPrAH as a coreactant; the ECL emission spectrum showed a peak at 467 nm with an ECL quantum efficiency of 0.39. Cheng and co-workers also found the ECL emission could be quenched via resonance energy transfer from the excited SCP Pdots to an acceptor. Figure 6b shows their proposed ECL emission mechanism of the SCP Pdots/TPrA system. Finally, Cheng and co-workers demonstrated a low-potential anodic ECL sensing strategy in which dopamine was the analyte and achieved a detection limit of 50 nM. These results suggest Pdots as an

alternative to Qdots as ECL emitters and point to the potential of using Pdots for developing low-potential ECL sensing systems.

Like ECL Pdots, chemiluminescent (CL) Pdots or CPNs do not require light excitation to generate emission. In CL Pdots or CPNs, the excitation energy is derived from redox reactions.[46,51,52,54] Wang and co-workers first studied CL in MEH-PPV CPNs functionalized with horseradish peroxidase, which formed a reaction system with luminol that was conjugated on the surface of CPNs and H_2O_2.[46] They found that, if the MEH-PPV CPNs were also doped with the photosensitizer meta-tetra (hydroxyphenyl)-chlorin (m-THPC), then there were two pathways for m-THPC to be excited by the CL system: One was directly through CL resonance energy transfer (CRET) and the other was through CRET and subsequent FRET. After this work, Kim and co-workers described a NIR nanoparticle that carried out aggregation-induced emission in which a green BODIPY dye was used as a relay molecule to bridge the energy gap between the AIE polymer (DPA-CN-PPV) and CL generated from H_2O_2-reacted peroxalates. Kim and co-workers demonstrated this nanocomposite could detect H_2O_2 in the 10^{-9} M concentration range and had high tissue penetration depth (>12 mm) under ex vivo conditions, which enabled them to perform deep imaging of inflammatory H_2O_2 in a hair-covered mouse model of peritonitis.[52]

Tang and co-workers fabricated the PFBT polymer covalently grafted with quaternary ammonium groups and the imidazopyriazinone moiety to form CL Pdots (Figure 6c), which exhibited high sensitivity down to the picomolar level in the detection of superoxide anion $(O_2^{\bullet})^-$. The CL Pdots had greatly prolonged luminescence time, enhanced specificity, and excellent biocompatibility.[51] Tang and co-workers' results show that, without exogenous stimulation, this probe was able to visualize in situ the differences in $O_2^{\bullet-}$ level between normal and tumor tissues of mice. They also applied the CL Pdots as energy acceptors for the sensitive imaging of intrinsic $O_2^{\bullet-}$ in mice based on CRET (Figure 6d). Recently, rather than using peroxalates as described above, Pu and co-workers prepared five types of bis(2,4,6-trichlorophenyl) oxalate containing semiconducting polymer nanoparticles with amplified CL for ultrasensitive in vivo imaging of reactive oxygen species.[54]

Both ECL Pdots and CL Pdots offer the distinct advantage that no light source is needed to generate emission. This greatly reduces background fluorescence interference and potential photodamage of the sample or probe.

AIE CPNs

In contrast to the commonly observed phenomenon of aggregation-caused quenching (ACQ) for most luminophores, aggregation-induced emission (AIE) is a phenomenon first described by Tang and co-workers.[97,98] In AIE, chromophores usually exhibit free molecular rotation in solution, which disrupts π-conjugation and prevents fluorescence emission. Aggregation prevents molecular rotation, thereby restoring π-conjugation to produce emission from the aggregated complex. Tang and co-workers have reported numerous AIE materials, including AIE-related conjugated polymers, which usually use tetraphenylethylene (TPE) as the AIE-active group and building block.[99] In addition to the pioneering work by Tang and co-workers, Li and co-workers reported AIE conjugated hyperbranched polymers, which were

synthesized by introducing TPE as the AIE-active group together with three other aromatic blocks.[55,56] They have studied the AIE of these polymers in THF/water mixed solution or in the film state and have applied them either as explosive chemosensors or incorporated them in various organic devices, but these AIE materials initially were not investigated with nanoparticle form.

Liu and co-workers prepared AIE CPNs by blending the conjugated polymer poly[9,9-bis(2-(2-(2-methoxyethoxy)-ethoxy)ethyl)fluorenyldivinylene] (PFV) with the AIE small-molecule emitter (2-(2,6-bis((*E*)-4-(phenyl(4′-(1,2,2-triphenyl-vinyl)-[1,1′-biphenyl]-4-yl)amino)styryl)-4*H*–pyran-4-ylidene)-malononitrile) (TPE-TPA-DCM) (Figure 7a). The AIE CPNs used bovine serum albumin (BSA) as the encapsulation matrix and exhibited size distribution from 125 to 159 nm in diameter. These AIE CPNs showed far-red/NIR emission through the excitation of the donor PFV and then energy transfer to the TPE-TPA-DCM AIE emitter (Figure 7b). Liu and co-workers found that the BSA matrix enabled further functionalization with the arginine-glycine-aspartic acid (RGD) peptide for specific recognition of the integrin receptor, which is overexpressed in cancer cells. They showed PFV amplified the emission from the TPE-TPA-DCM AIE chromophore and carried out imaging experiments using HT-29 colon cancer cells as well as a hepatoma-bearing mouse model (Figure 7c).

Rather than blending conjugated polymers with AIE emitters, the Tang group and Zhu group have obtained AIE CPNs via dispersion polymerization using geminal cross-coupling of 1,1-dibromoolefins and reported different particle sizes ranging from 147 to 1047 nm in diameter.[59] Kim and co-workers have prepared DPA-CN-PPV AIE-active nanoparticles for in vivo CL sensing as discussed in the previous section.[52] The Wang group developed two types of AIE CPNs made from polymers synthesized via Suzuki polymerization and Pd-catalyzed Sonogashira reaction, respectively.[58,60] In one of these works,[58] monomers of boron ketoiminate derivatives were used as the AIE-active fluorophore, which was polymerized with fluorene monomers (Figure 7d). The AIE CPNs were then prepared through reprecipitation from these conjugated polymers, with particle diameters ranging from 85 to 95 nm. These AIE CPNs showed low cytotoxicity and good photostability and were applied for cell imaging (Figure 7e).

DUAL-MODAL Pdots AND CPNs

Given the interest in multimodality in vivo imaging, Pdots[62] and CPNs that offer dual-modal imaging capabilities have been developed.[63–65] For example, Rao and co-workers reported on CPNs for dual-mode fluorescence and photoacoustic imaging.[63] Here, CPNs with NIR light absorbing polymers were doped with NIR775 dyes. In terms of the photoacoustic signal, these CPNs were shown to offer stronger signals than single-walled carbon nanotubes and gold nanorods on a per mass basis. The CPNs allowed whole-body lymph-node photoacoustic mapping in mice at a low systemic injection mass concentration. Additionally, the CPNs possessed narrow photoacoustic spectral profiles and resistance to photodegradation and oxidation, which enabled their further development into NIR ratiometric photoacoustic probe for in vivo real-time imaging of reactive oxygen species (Figure 8).

Pdots for dual-mode fluorescence and magnetic resonance imaging (MRI) have also been reported. Green and co-workers described Pdots of ~30 nm diameter, prepared from hydrophobic conjugated polymers, amphiphilic phospholipids, and a Gd-containing lipid.[62] They characterized the fluorescence quantum yield, extinction coefficient, and the MRI T1-weighted relaxation times for the MRI-active Pdot. They then applied these Pdots for cellular imaging using confocal microscopy and demonstrated that the Pdots generate a linear relationship between T1-weighted relaxation rates and the Gd concentrations. Our group also developed Pdots incorporating either Au or iron oxide nanoparticles to create dual-mode (e.g., for fluorescence and dark-field imaging) or dual-functional (e.g., magnetic and fluorescence) Pdots.[100] In summary, all these studies suggest Pdots and CPNs represent a promising platform for developing a multifunctional probe for multimodal microscopy, especially for in vivo imaging.

Pdots AND CPNs AS BIOSENSORS

A Pdot is well-suited for the development of biosensors because of its high brightness and efficient modulation by small-molecule sensors through energy transfer. We and others have reported on many types of Pdot and CPN sensors.[66–81] For example, we have reported on Pdot sensors for pH, Cu^{2+}/Fe^{2+} ions, and temperature.[101–103]

Chen and his co-workers have applied PFO CPNs to detect carcinoembryonic antigen (CEA) with high sensitivity based on FRET between CPNs and Au NP; they reported a proportional increase in fluorescence intensity as a function of CEA concentration in the range of 0.1–10 ng mL^{-1}.[66] Wu and co-workers used terbium-chelated PFO Pdots to detect bacterial spores in a ratiometric fashion.[67] Zhang and his co-workers detected and imaged bacteria with PFBT CPNs,[70] based on FRET between PFO Pdots and a metal organic framework. Weng and co-workers explored sensing using protease (MMP-2) and PFO CPNs.[71] Moon and co-workers applied four different CPNs to differentiate structurally similar glycosaminoglycans (GAGs) in a urine simulant.[73] Tang and co-workers described CPNs for selective detection of HOCl.[74] For detecting fluoride ions, Chan and co-workers described a ratiometric fluorescent Pdot sensor, and Huang and co-workers reported on a dual-emission Pdot sensor.[69,75] Wang and co-workers have found that CPNs displayed high selectivity and sensitivity for Fe(III) ions in water because of aggregation-induced fluorescence quenching between Pdots and Fe(III) ion.[77] Gao and co-workers demonstrated sensing and imaging of tyrosinase activity using two-photon excited Pdots (PFO/ CN-PPV) with dual emission,[78] and together with the Wang group, they also developed PFBT Pdots for turn-on sensing of phytic acid.[80] Chen and co-workers doped two different dyes, fluorescein isothiocyanate (FITC) and Pt(II) meso-tetra-(pentafluorophenyl)porphine, into PFO Pdots to simultaneous image intracellular pH and O_2.[81] Chan and co-workers developed two types of Pdots for ratiometric sensing of Cu^{2+} ion[68] and Pb^{2+} ion.[72] In this latter work, they also reported on a sensitive approach for Pb^{2+} sensing based on a new type of PFBT Pdot capped and functionalized with polydiacetylenes; the signals were visible to the naked eye, which motivated Chan and co-workers to prepare an easy-to-read test strip for field use.

Huang and co-workers prepared a dual-emissive conjugated polyelectrolyte by introducing platinum(II) porphyrin with O_2-sensitive phosphorescent into a fluorene-based conjugated

polyelectrolyte with O_2-insensitive blue fluorescence. These conjugated polyelectrolytes formed very small nanoparticles in PBS buffer via self-assembly. Huang and co-workers applied them to O_2 sensing for imaging and studying tumor hypoxia in a mouse model.

The above sensors were mostly for detecting ions or small gaseous molecules like O_2 in biological environments. However, the sensing of larger biological molecules has been more elusive. Recently, Wu and co-workers reported on a new Pdot sensing platform for biomolecules, such as glucose. They used the oxygen consuming enzymes (glucose oxidase (GOx)) as the molecular recognition element for glucose; this GOx was conjugated on the surface of Pdots, which contained the oxygen-sensitive dye (PtOEP) in their interior.[79] In this way, Pdot acted as a transduction element that converted the output of GOx into a ratiometric optical signal. Wu and co-workers showed this Pdot-GOx sensor had high sensitivity and excellent selectivity with tunable dynamic range (Figure 9a–d). They also conducted long-term continuous glucose monitoring (Figure 9e–h) by implanting the sensor in mice. This strategy should open new opportunities in the development of Pdot biosensors for biologically important molecules, such as metabolites and drugs.

Pdots FOR PHOTODYNAMIC THERAPY

Photodynamic therapy (PDT) as a minimally invasive approach for treatment of various malignant cancers and other diseases has been investigated for several decades.[104] In a typical PDT process, three primary components are involved: light irradiation, photosensitizer, and molecular oxygen. Excitation of the photosensitizer converts oxygen in its ground state to singlet oxygen, which efficiently and locally attacks the cells and tissues exposed to light, ideally with no or minimal damage to the surrounding tissue. The photosensitizer plays an essential role in the development and application of modern PDT treatment. Common photosensitizers include porphyrin, chlorin, and their derivatives.

Pdots offer an attractive platform for PDT because of their large extinction coefficients. Indeed, in recent years, several groups have described Pdot-based photosensitizers for PDT.[82–86] For example, Huang and co-workers reported a series of Pdots prepared via conjugating the phosphorescent Ir(III) complex with polyfluorene units in the conjugated polymer chain. These Pdots possessed good photostability, biocompatibility, and efficient energy transfer from polyfluorene to the Ir(III)complex. The energy transfer in the triplet–triplet annihilation process enabled efficient singlet oxygen generation, causing effective killing and initiating apoptosis of cancer cells upon light irradiation.[82]

In another work by the same group, a Pdot-based photosensitizer was developed by conjugating Pt(II) porphyrin as an oxygen-responsive phosphorescent group (hydrophobic) into a polyfluorene-based hyperbranched conjugated polyelectrolyte (amphiphilic),[86] after which the amphiphilic conjugated polymer chains self-assembled into a nanoparticle form (Figure 10a). Huang and co-workers found that the Pt(II) complex containing Pdots have ratiometric luminescence: fluorescence from polyfluorene and phosphorescence from Pt(II) complexes for sensing oxygen. They quantified O_2 by measuring the ratiometric emission intensity of phosphorescence and fluorescence as well as from the lifetime of phosphorescence. In their intracellular hypoxia measurement, Huang and co-workers

showed cells treated with Pdots displayed longer lifetimes under hypoxic conditions, and time-resolved luminescence images showed a higher S/N ratio after gating off the short-lived background fluorescence. Finally, the PDT efficiency of the Pdots was estimated by flow cytometry, a cell-viability assay, and in situ imaging of PDT-induced cell death.

The Wu group and Xu group collaborated to demonstrate the amplified singlet oxygen generation in a Pdot-based photosensitizer for PDT.[83,84] Here, tetraphenylporphyrin (TPP) was doped in or conjugated to PFBT Pdots. In their latter work, the TPP monomers were covalently incorporated into the PFBT π-conjugated backbone to form PFBT-TPP Pdots. These Pdots showed excellent stability, which addressed the potential concern of leakage of the TPP photosensitizer from the TPP-doped Pdots. Furthermore, these PFBT-TPP Pdots showed a high $^1O_2$ generation quantum yield of 35% and low dark toxicity. They evaluated the cytotoxicity and photodynamic effects of the PFBT-TPP Pdot in MCF-7 cells, which indicated that the PFBT-TPP Pdots could efficiently kill cancer cells because of their high-yield of $^1O_2$ generation. The two groups also investigated the therapeutic efficacy of the Pdots in vivo with tumor-bearing mice. By monitoring the tumor growth rate in mice receiving intratumoral Pdot injections and light irradiation, they found the tumors were significantly inhibited or eradicated in certain cases (Figure 10b–g), which points to these Pdots' potential for use as a new generation of PDT agents.

Other conjugated-polymer-based nanoparticles have been recently implemented in photoacoustic/photothermal therapy, as reported by the Rao, Pu, and other research groups.[85,105–108] These nanoparticles, however, either tend to contain too little fluorescent conjugated polymer to be classified as Pdots (or CPNs) or do not have dynamics involved in the whole therapeutic process to be regarded as PDT. As a result, we will not review them here.

ADDITIONAL CONSIDERATIONS AND SUMMARY

While we highlighted recent work in developing and applying different types of Pdots and CPNs, we note there is a large body of work devoted to improving the performance of Pdots and CPNs. The work includes efforts to tune the photophysical properties of Pdots/CPNs,[109–114] decrease the nonspecific binding of Pdots,[115] expand their biological applications,[73,116,117] and build hybrid nanostructures for imaging cancer cells.[118] Additionally, our group developed a lyophilization process for Pdot bioconjugates, which we hope will facilitate their use by the biomedical community.[61] Fundamental studies of Pdots and CPNs, especially their photophysical properties, are also ongoing, including recent reports by the McNeill group[119–122] and by other research groups.[94,123–125] There have also been many reports on the development and application of different Pdots and CPNs as imaging or tracking probes.[27,78,94,109,125–130]

The remarkable productivity of this area in the past several years since our last review has further highlighted the potential impact Pdots may have in biology and medicine. However, despite the rapid advances made in the past few years, much remains to be done to further refine Pdots into robust and consistent probes for daily use by the biomedical researchers. We anticipate this field to continue its rapid development in the coming three to five years.

During this time, we fully expect some Pdots will enable life-science researchers to ask new and more sophisticated questions.

Acknowledgments

We are grateful to the National Institutes of Health (CA186798) and the University of Washington for support of this work.

Biographies

Jiangbo Yu obtained his Ph.D. degree in Chemistry from the Chinese Academy of Sciences (CAS) in 2005 and has since then worked as Associated Professor in Changchun Institute of Applied Chemistry, CAS. In 2007, he went to the University of Regensburg (Germany) and worked as a research assistant. From 2008 to 2011, he worked as a postdoctoral researcher at Clemson University. Since 2011, he has worked as a Senior Research Scientist in the Department of Chemistry, University of Washington. His current research interest focuses on designing and developing fluorescent nanoprobes for biology and studying the photophysical properties of probes by single molecule spectroscopy/imaging and other bioanalytical techniques.

Yu Rong received his B.S. and Ph.D. from Zhejiang University, P.R.China. He has been Senior Research Scientist in Prof. Daniel Chiu's group at the Department of Chemistry, University of Washington since 2014. His work has involved the design and synthesis of new conjugated polymers and development of fluorescent nanoparticles for biological applications.

Chun-Ting Kuo received his B.S. and M.S. degrees from National Tsing Hua University (Taiwan), as well as his Ph.D. degree from National Taiwan University (Taiwan). He worked as a postdoctoral research associate at National Taiwan University and the University of Washington. Now, he is a research scientist in the University of Washington. His research interests involve high performance liquid chromatography, the synthesis and size control of gold nanoparticles, employing gold nanoparticles as sensing probes, and *I-V* characteristics of single-molecule transistors. He has recently worked on fluorescent nanoparticles for biomedical applications.

Xing-Hua Zhou received a Ph.D. in organic chemistry from Peking University in 2005. Since graduating, he has been working at the University of Washington in Seattle as a postdoctoral research associate, acting instructor, and research scientist. His research interests are focused on development of organic and polymeric semiconducting functional materials and their nanomaterials (polymer dots) for optoelectronic, photonic, biological, and medical applications.

Daniel T. Chiu is currently the A. Bruce Montgomery Professor of Chemistry and Professor of Bioengineering at the University of Washington. His research is focused on developing new methods based on nanotechnology and nanomaterials for probing biological processes at the single-cell and single-molecule level and on applying these new techniques for addressing pressing biomedical problems.

References

1. Kelly TL, Wolf MO. Chem. Soc. Rev. 2010; 39(5):1526–1535. [PubMed: 20419207]
2. Pecher J, Mecking S. Chem. Rev. (Washington, DC, U. S.). 2010; 110(10):6260–6279.
3. Tian Z, Yu J, Wu C, Szymanski C, McNeill J. Nanoscale. 2010; 2(10):1999–2011. [PubMed: 20697652]
4. Tuncel D, Demir HV. Nanoscale. 2010; 2(4):484–494. [PubMed: 20644748]
5. Li K, Liu B. J. Mater. Chem. 2012; 22(4):1257–1264.
6. Li Y, Li K, Liu B. RSC Polym. Chem. Ser. 2012; 2:399–423. (Molecular Design and Applications of Photofunctional Polymersand Materials).
7. Feng L, Zhu C, Yuan H, Liu L, Lv F, Wang S. Chem. Soc. Rev. 2013; 42(16):6620–6633. [PubMed: 23744297]
8. Fischer I, Kaeser A, Peters-Gumbs MAM, Schenning APH. J. Chem. - Eur. J. 2013; 19(33):10928–10934.
9. Sun W, Yu J, Ye F, Rong Y, Chiu DT. Proc. SPIE. 2013; 8812 (Biosensing and NanomedicineVI), 881205-1-881205-9.
10. Tang R, Feng X. Can. Chem. Trans. 2013; 1(1):78–84.
11. Wu C, Chiu DT. Angew. Chem., Int. Ed. 2013; 52(11):3086–3109.
12. Li K, Liu B. Chem. Soc. Rev. 2014; 43(18):6570–6597. [PubMed: 24792930]
13. Xu H, Li Q, Wang L, He Y, Shi J, Tang B, Fan C. Chem. Soc. Rev. 2014; 43(8):2650–2661. [PubMed: 24394966]
14. Chan Y-H, Wu P-J. Part. Part. Syst. Charact. 2015; 32(1):11–28.
15. Dhand C, Dwivedi N, Loh XJ, Jie Ying AN, Verma NK, Beuerman RW, Lakshminarayanan R, Ramakrishna S. RSC Adv. 2015; 5(127):105003–105037.
16. Massey M, Wu M, Conroy EM, Algar WR. Curr. Opin. Biotechnol. 2015; 34:30–40. [PubMed: 25481436]
17. Peng H-S, Chiu DT. Chem. Soc. Rev. 2015; 44(14):4699–4722. [PubMed: 25531691]
18. Wolfbeis OS. Chem. Soc. Rev. 2015; 44(14):4743–4768. [PubMed: 25620543]
19. Pu K, Chattopadhyay N, Rao J. J. Controlled Release. 2016; 240:312.
20. Ye F, White CC, Jin Y, Hu X, Hayden S, Zhang X, Gao X, Kavanagh TJ, Chiu DT. Nanoscale. 2015; 7(22):10085–10093. [PubMed: 25978523]
21. Rong Y, Wu C, Yu J, Zhang X, Ye F, Zeigler M, Gallina ME, Wu IC, Zhang Y, Chan Y-H, Sun W, Uvdal K, Chiu DT. ACS Nano. 2013; 7(1):376–384. [PubMed: 23282278]
22. Sun W, Yu J, Deng R, Rong Y, Fujimoto B, Wu C, Zhang H, Chiu DT. Angew. Chem., Int. Ed. 2013; 52(43):11294–11297.
23. Zhang X, Yu J, Rong Y, Ye F, Chiu DT, Uvdal K. Chem. Sci. 2013; 4(5):2143–2151. [PubMed: 28959389]
24. Li Q, Zhang J, Sun W, Yu J, Wu C, Qin W, Chiu DT. Langmuir. 2014; 30(28):8607–8614. [PubMed: 24976495]
25. Rong Y, Yu J, Zhang X, Sun W, Ye F, Wu IC, Zhang Y, Hayden S, Zhang Y, Wu C, Chiu DT. ACS Macro Lett. 2014; 3(10):1051–1054. [PubMed: 25419486]
26. Wu IC, Yu J, Ye F, Rong Y, Gallina ME, Fujimoto BS, Zhang Y, Chan Y-H, Sun W, Zhou X-H, Wu C, Chiu DT. J. Am. Chem. Soc. 2015; 137(1):173–178. [PubMed: 25494172]
27. Xiong L, Shuhendler AJ, Rao J. Nat. Commun. 2012; 3:1193. [PubMed: 23149738]
28. Chen C-P, Huang Y-C, Liou S-Y, Wu P-J, Kuo S-Y, Chan Y-H. ACS Appl. Mater. Interfaces. 2014; 6(23):21585–21595. [PubMed: 25394668]
29. Hong G, Zou Y, Antaris AL, Diao S, Wu D, Cheng K, Zhang X, Chen C, Liu B, He Y, Wu JZ, Yuan J, Zhang B, Tao Z, Fukunaga C, Dai H. Nat. Commun. 2014; 5:4206. [PubMed: 24947309]
30. Wu P-J, Kuo S-Y, Huang Y-C, Chen C-P, Chan Y-H. Anal. Chem. (Washington, DC, U. S.). 2014; 86(10):4831–4839.
31. Liu H-Y, Wu P-J, Kuo S-Y, Chen C-P, Chang E-H, Wu C-Y, Chan Y-H. J. Am. Chem. Soc. 2015; 137(32):10420–10429. [PubMed: 26255823]

32. Palner M, Pu K, Shao S, Rao J. Angew. Chem., Int. Ed. 2015; 54(39):11477–11480.
33. Xiong L, Cao F, Cao X, Guo Y, Zhang Y, Cai X. Bioconjugate Chem. 2015; 26(5):817–821.
34. Liou S-Y, Ke C-S, Chen J-H, Luo Y-W, Kuo S-Y, Chen Y-H, Fang C-C, Wu C-Y, Chiang C-M, Chan Y-H. ACS Macro Lett. 2016; 5(1):154–157.
35. Xiong L, Guo Y, Zhang Y, Cao F. J. Mater. Chem. B. 2016; 4(2):202–206.
36. Ye F, Wu C, Sun W, Yu J, Zhang X, Rong Y, Zhang Y, Wu IC, Chan Y-H, Chiu DT. Chem. Commun. (Cambridge, U. K.). 2014; 50(42):5604–5607.
37. Ye F, Sun W, Zhang Y, Wu C, Zhang X, Yu J, Rong Y, Zhang M, Chiu DT. Langmuir. 2015; 31(1): 499–505. [PubMed: 25521606]
38. Chan Y-H, Gallina ME, Zhang X, Wu IC, Jin Y, Sun W, Chiu DT. Anal. Chem. (Washington, DC, U. S.). 2012; 84(21):9431–9438.
39. Osakada Y, Hanson L, Cui B. Chem. Commun. (Cambridge, U. K.). 2012; 48(27):3285–3287.
40. Chen J, Wang D, Turshatov A, Munoz-Espi R, Ziener U, Koynov K, Landfester K. Polym. Chem. 2013; 4(3):773–781.
41. Kuo C-T, Thompson AM, Gallina ME, Ye F, Johnson ES, Sun W, Zhao M, Yu J, Wu IC, Fujimoto B, DuFort CC, Carlson MA, Hingorani SR, Paguirigan AL, Radich JP, Chiu DT. Nat. Commun. 2016; 7:11468. [PubMed: 27118210]
42. Talbert W, Jones D, Morimoto J, Levine M. New J. Chem. 2016; 40(9):7273–7277.
43. Zhang X, Chamberlayne CF, Harbron EJ, Kurimoto A, Frank NL. Chem. Commun. (Cambridge, U. K.). 2016; 52(22):4144–7.
44. Palacios RE, Fan F-RF, Grey JK, Suk J, Bard AJ, Barbara PF. Nat. Mater. 2007; 6(9):680–685. [PubMed: 17643107]
45. Chang Y-L, Palacios RE, Fan F-RF, Bard AJ, Barbara PF. J. Am. Chem. Soc. 2008; 130(28):8906–8907. [PubMed: 18572939]
46. Zhang Y, Pang L, Ma C, Tu Q, Zhang R, Saeed E, Mahmoud AE, Wang J. Anal. Chem. 2014; 86(6):3092–3099. [PubMed: 24552272]
47. Dai R, Wu F, Xu H, Chi Y. ACS Appl. Mater. Interfaces. 2015; 7(28):15160–15167. [PubMed: 26115552]
48. Lu Q, Zhang J, Wu Y, Chen S. RSC Adv. 2015; 5(78):63650–63654.
49. Chen H, Lu Q, Liao J, Yuan R, Chen S. Chem. Commun. (Cambridge, U. K.). 2016; 52(45):7276–7279.
50. Feng Y, Lei J, Ju H, Dai C, Cheng Y. Anal. Chem. 2016; 88(1):845–50. [PubMed: 26613322]
51. Li P, Liu L, Xiao H, Zhang W, Wang L, Tang B. J. Am. Chem. Soc. 2016; 138(9):2893–2896. [PubMed: 26908223]
52. Seo YH, Singh A, Cho H-J, Kim Y, Heo J, Lim C-K, Park SY, Jang W-D, Kim S. Biomaterials. 2016; 84:111–118. [PubMed: 26826300]
53. Wu F, Feng Y, Chi YJ. Electroanal. Chem. 2016; 779:47–54.
54. Zhen X, Zhang C, Xie C, Miao Q, Lim KL, Pu K. ACS Nano. 2016; 10(6):6400–6409. [PubMed: 27299477]
55. Wu W, Ye S, Huang L, Xiao L, Fu Y, Huang Q, Yu G, Liu Y, Qin J, Li Q, Li Z. J. Mater. Chem. 2012; 22(13):6374–6382.
56. Wu W, Ye S, Yu G, Liu Y, Qin J, Li Z. Macromol. Rapid Commun. 2012; 33(2):164–171. [PubMed: 22134953]
57. Ding D, Li K, Qin W, Zhan R, Hu Y, Liu J, Tang BZ, Liu B. Adv. Healthcare Mater. 2013; 2(3): 500–507.
58. Dai C, Yang D, Fu X, Chen Q, Zhu C, Cheng Y, Wang L. Polym. Chem. 2015; 6(28):5070–5076.
59. Chen T, Yin H, Chen Z-Q, Zhang G-F, Xie N-H, Li C, Gong W-L, Tang BZ, Zhu M-Q. Small. 2016; doi: 10.1002/smll.201601410
60. Yang D, Li F, Luo Z, Bao B, Hu Y, Weng L, Cheng Y, Wang L. J. Polym. Sci., Part A: Polym. Chem. 2016; 54(12):1686–1693.
61. Sun W, Ye F, Gallina ME, Yu J, Wu C, Chiu DT. Anal. Chem. (Washington, DC, U. S.). 2013; 85(9):4316–4320.

62. Hashim Z, Green M, Chung PH, Suhling K, Protti A, Phinikaridou A, Botnar R, Khanbeigi RA, Thanou M, Dailey LA, Commander NJ, Rowland C, Scott J, Jenner D. Nanoscale. 2014; 6(14): 8376–8386. [PubMed: 24941427]
63. Pu K, Shuhendler AJ, Jokerst JV, Mei J, Gambhir SS, Bao Z, Rao J. Nat. Nanotechnol. 2014; 9(3): 233–239. [PubMed: 24463363]
64. Cui L, Rao J. Wiley Interdiscip Rev. Nanomed Nanobiotechnol. 2016; doi: 10.1002/wnan.1418
65. Shan Y, Panday N, Myoung Y, Twomey M, Wang X, Li W, Celik E, Moy V, Wang H, Moon JH, He J. Macromol. Biosci. 2016; 16(4):599–607. [PubMed: 26757346]
66. Lin Z, Zhang G, Yang W, Qiu B, Chen G. Chem. Commun. (Cambridge, U. K.). 2012; 48(79): 9918–9920.
67. Li Q, Sun K, Chang K, Yu J, Chiu DT, Wu C, Qin W. Anal. Chem. (Washington, DC, U. S.). 2013; 85(19):9087–9091.
68. Wu P-J, Chen J-L, Chen C-P, Chan Y-H. Chem. Commun. (Cambridge, U. K.). 2013; 49(9):898–900.
69. Huang Y-C, Chen C-P, Wu P-J, Kuo S-Y, Chan Y-H. J. Mater. Chem. B. 2014; 2(37):6188–6191.
70. Wan Y, Zheng L, Sun Y, Zhang D. J. Mater. Chem. B. 2014; 2(30):4818–4825.
71. Yang W, Zhang G, Weng W, Qiu B, Guo L, Lin Z, Chen G. RSC Adv. 2014; 4(102):58852–58857.
72. Kuo S-Y, Li H-H, Wu P-J, Chen C-P, Huang Y-C, Chan Y-H. Anal. Chem. (Washington, DC, U. S.). 2015; 87(9):4765–4771.
73. Twomey M, Vokata T, Kumar MR, Moon JH. Chem. Commun. (Cambridge, U. K.). 2015; 51(19): 4065–4068.
74. Wang H, Li Y, Chen Y, Li L, Fang T, Tang Z. J. Mater. Chem. C. 2015; 3(20):5136–5140.
75. Zhao Q, Zhang C, Liu S, Liu Y, Zhang KY, Zhou X, Jiang J, Xu W, Yang T, Huang W. Sci. Rep. 2015; 5:16420. [PubMed: 26552859]
76. Zhao Q, Zhou X, Cao T, Zhang KY, Yang L, Liu S, Liang H, Yang H, Li F, Huang W. Chem. Sci. 2015; 6(3):1825–1831. [PubMed: 28694947]
77. Feng L, Guo L, Wang X. Biosens. Bioelectron. 2017; 87:514–521. [PubMed: 27598853]
78. Sun J, Mei H, Wang S, Gao F. Anal. Chem. (Washington, DC, U. S.). 2016; 88(14):7372–7377.
79. Sun K, Tang Y, Li Q, Yin S, Qin W, Yu J, Chiu DT, Liu Y, Yuan Z, Zhang X, Wu C. ACS Nano. 2016; 10(7):6769–6781. [PubMed: 27303785]
80. Wang C, Sun J, Mei H, Gao F. Anal. Methods. 2016; 8:7755–7761.
81. Xu W, Lu S, Xu M, Jiang Y, Wang Y, Chen X. J. Mater. Chem. B. 2016; 4(2):292–298.
82. Shi H, Ma X, Zhao Q, Liu B, Qu Q, An Z, Zhao Y, Huang W. Adv. Funct. Mater. 2014; 24(30): 4823–4830.
83. Chang K, Tang Y, Fang X, Yin S, Xu H, Wu C. Biomacromolecules. 2016; 17(6):2128–2136. [PubMed: 27219282]
84. Li S, Chang K, Sun K, Tang Y, Cui N, Wang Y, Qin W, Xu H, Wu C. ACS Appl. Mater. Interfaces. 2016; 8(6):3624–3634. [PubMed: 26492203]
85. Zhang D, Wu M, Zeng Y, Liao N, Cai Z, Liu G, Liu X, Liu J. J. Mater. Chem. B. 2016; 4(4):589–599.
86. Zhou X, Liang H, Jiang P, Zhang KY, Liu S, Yang T, Zhao Q, Yang L, Lv W, Yu Q, Huang W. Adv. Sci. (Weinheim, Ger.). 2016; 3(2):1500155.
87. Kowada T, Maeda H, Kikuchi K. Chem. Soc. Rev. 2015; 44(14):4953–4972. [PubMed: 25801415]
88. Yu J, Wu C, Zhang X, Ye F, Gallina ME, Rong Y, Wu IC, Sun W, Chan Y-H, Chiu DT. Adv. Mater. 2012; 24(26):3498–504. [PubMed: 22684783]
89. Bunzli J-CG. Chem. Rev. 2010; 110(5):2729–2755. [PubMed: 20151630]
90. Jin Y, Ye F, Zeigler M, Wu C, Chiu DT. ACS Nano. 2011; 5(2):1468–1475. [PubMed: 21280613]
91. Binnemans K. Chem. Rev. 2009; 109(9):4283–4374. [PubMed: 19650663]
92. Aitasalo T, Deren P, Holsa J, Jungner H, Krupa JC, Lastusaari M, Legendziewicz J, Niittykoski J, Strek W. J. Solid State Chem. 2003; 171(1–2):114–122.
93. Aubin JE. J. Histochem. Cytochem. 1979; 27(1):36–43. [PubMed: 220325]

94. Sun K, Chen H, Wang L, Yin S, Wang H, Xu G, Chen D, Zhang X, Wu C, Qin W. ACS Appl. Mater. Interfaces. 2014; 6(13):10802–10812. [PubMed: 24930393]
95. Ye F, Wu C, Jin Y, Wang M, Chan Y-H, Yu J, Sun W, Hayden S, Chiu DT. Chem. Commun. (Cambridge, U. K.). 2012; 48(12):1778–1780.
96. Wu C, Schneider T, Zeigler M, Yu J, Schiro PG, Burnham DR, McNeill JD, Chiu DT. J. Am. Chem. SoC. 2010; 132(43):15410–15417. [PubMed: 20929226]
97. Luo J, Xie Z, Lam JWY, Cheng L, Chen H, Qiu C, Kwok HS, Zhan X, Liu Y, Zhu D, Tang BZ. Chem. Commun. (Cambridge, U. K.). 2001; 18:1740–1741.
98. Mei J, Leung NLC, Kwok RTK, Lam JWY, Tang BZ. Chem. Rev. 2015; 115(21):11718–11940. [PubMed: 26492387]
99. Hu R, Maldonado JL, Rodriguez M, Deng C, Jim CKW, Lam JWY, Yuen MMF, Ramos-Ortiz G, Tang BZ. J. Mater. Chem. 2012; 22(1):232–240.
100. Sun W, Hayden S, Jin Y, Rong Y, Yu J, Ye F, Chan Y-H, Zeigler M, Wu C, Chiu DT. Nanoscale. 2012; 4(22):7246–7249. [PubMed: 23072832]
101. Chan Y-H, Jin Y, Wu C, Chiu DT. Chem. Commun. 2011; 47(10):2820–2822.
102. Chan Y-H, Wu C, Ye F, Jin Y, Smith PB, Chiu DT. Anal. Chem. 2011; 83(4):1448–1455. [PubMed: 21244093]
103. Ye F, Wu C, Jin Y, Chan Y-H, Zhang X, Chiu DT. J. Am. Chem. SoC. 2011; 133(21):8146–8149. [PubMed: 21548583]
104. Dolmans DEJGJ, Fukumura D, Jain RK. Nat. Rev. Cancer. 2003; 3(5):380. [PubMed: 12724736]
105. Zhang Y, Pang L, Ma C, Tu Q, Zhang R, Saeed E, Mahmoud AE, Wang J. Anal. Chem. (Washington, DC, U. S.). 2014; 86(6):3092–3099.
106. Pu K, Mei J, Jokerst JV, Hong G, Antaris AL, Chattopadhyay N, Shuhendler AJ, Kurosawa T, Zhou Y, Gambhir SS, Bao Z, Rao J. Adv. Mater. (Weinheim, Ger.). 2015; 27(35):5184–5190.
107. Lyu Y, Fang Y, Miao Q, Zhen X, Ding D, Pu K. ACS Nano. 2016; 10(4):4472–4481. [PubMed: 26959505]
108. Lyu Y, Xie C, Chechetka SA, Miyako E, Pu K. J. Am. Chem. SoC. 2016; 138:9049. [PubMed: 27404507]
109. Chen C-P, Wu P-J, Liou S-Y, Chan Y-H. RSC Adv. 2013; 3(38):17507–17514.
110. Zhang Y, Yu J, Gallina ME, Sun W, Rong Y, Chiu DT. Chem. Commun. (Cambridge, U. K.). 2013; 49(74):8256–8258.
111. Kim BS-I, Jin Y-J, Lee W-E, Byun DJ, Yu R, Park S-J, Kim H, Song K-H, Jang S-Y, Kwak G. Adv. Opt. Mater. 2015; 3(1):78–86.
112. Zhang Y, Ye F, Sun W, Yu J, Wu IC, Rong Y, Zhang Y, Chiu DT. Chemical Science. 2015; 6(3): 2102–2109. [PubMed: 25709806]
113. Narasimha K, Jayakannan M. Macromolecules (Washington, DC, U. S.). 2016; 49(11):4102–4114.
114. Yang C, Liu H, Zhang Y, Xu Z, Wang X, Cao B, Wang M. Biomacromolecules. 2016; 17(5): 1673–1683. [PubMed: 27010718]
115. Koner AL, Krndija D, Hou Q, Sherratt DJ, Howarth M. ACS Nano. 2013; 7(2):1137–1144. [PubMed: 23330847]
116. Mendez E, Moon JH. Chem. Commun. (Cambridge, U. K.). 2013; 49(54):6048–6050.
117. Li S, Chen J, Chen G, Li Q, Sun K, Yuan Z, Qin W, Xu H, Wu C. Macromol. Biosci. 2015; 15(3): 318–327. [PubMed: 25504417]
118. Noh J, Kim D, Jang G, Kim J, Heo MB, Lee N-E, Kim C-Y, Lee E, Kim Y-J, Lim YT, Lee TS. RSC Adv. 2014; 4(78):41378–41386.
119. Groff LC, Wang X, McNeill JD. J. Phys. Chem. C. 2013; 117(48):25748–25755.
120. Tian Z, Yu J, Wang X, Groff LC, Grimland JL, McNeill JD. J. Phys. Chem. B. 2013; 117(16): 4517–4520. [PubMed: 23214470]
121. Wang L, Wu C-F, Wang H-Y, Wang Y-F, Chen Q-D, Han W, Qin W-P, McNeill J, Sun H-B. Nanoscale. 2013; 5(16):7265–7270. [PubMed: 23817864]
122. Wang X, Groff LC, McNeill JD. Langmuir. 2013; 29(45):13925–13931. [PubMed: 24099661]

123. Mandal S, Bhattacharyya S, Borovkov V, Patra A. J. Phys. Chem. C. 2012; 116(20):11401–11407.

124. Martin C, Bhattacharyya S, Patra A, Douhal A. Photochem. Photobiol. Sci. 2014; 13(9):1241–1252. [PubMed: 24969364]

125. Peters M, Zaquen N, D'Olieslaeger L, Bove H, Vanderzande D, Hellings N, Junkers T, Ethirajan A. Biomacromolecules. 2016; 17(8):2562–2571. [PubMed: 27345494]

126. Adkins CT, Dobish JN, Brown S, Harth E. ACS Macro Lett. 2013; 2(8):710–714. [PubMed: 24516779]

127. Pu K, Shuhendler AJ, Valta MP, Cui L, Saar M, Peehl DM, Rao J. Adv. Healthcare Mater. 2014; 3(8):1292–1298.

128. He T, Hu W, Shi H, Pan Q, Ma G, Huang W, Fan Q, Lin X. Dyes Pigm. 2015; 123:218–221.

129. Zhang W, Sun H, Yin S, Chang J, Li Y, Guo X, Yuan ZJ. Mater. Sci. 2015; 50(16):5571–5577.

130. Twomey M, Mendez E, Manian RK, Lee S, Moon JH. Chem. Commun. (Cambridge, U. K.). 2016; 52(27):4910–4913.

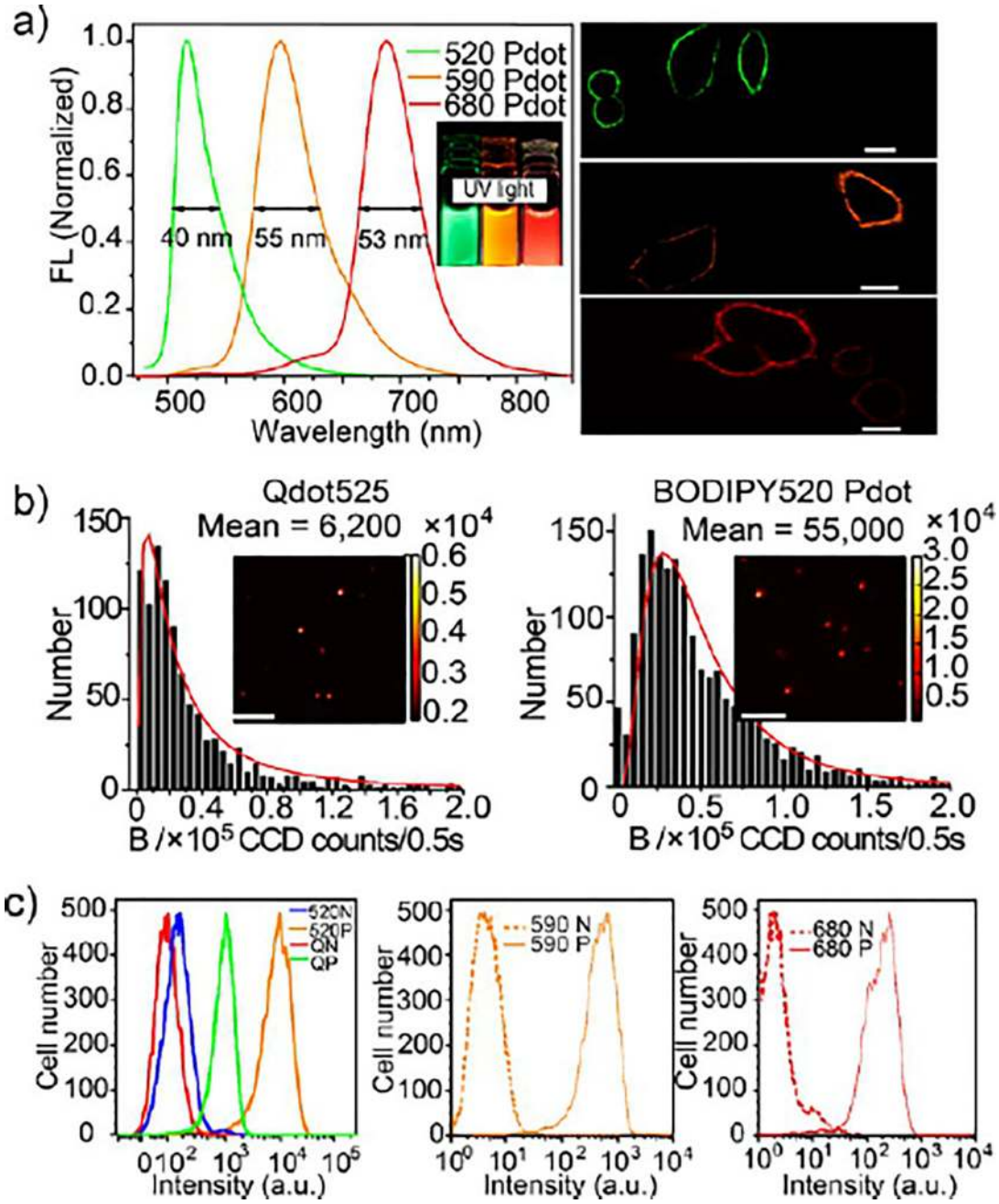

Figure 1.

(a) Left panel, fluorescence emission spectra of BODIPY 520 Pdots (λ_{ex} = 405 nm), BODIPY 590 Pdots, and BODIPY 680 Pdots (λ_{ex} = 450 nm); right panel, confocal fluorescence microscopy images of MCF-7 cells labeled with BODIPY 520 Pdot-SA, BODIPY 600 Pdot-SA, and BODIPY 690 Pdot-SA; scale bars: 20 mm. (b) Histograms of the distributions of single-particle brightness of Qdots 525 and BODIPY 520 Pdots (λ_{ex} = 405 nm). The red curves were obtained by fitting a log-normal distribution to the histogram and gave 6200 and 55000 mean CCD counts, respectively. Insets: single-particle brightness images were obtained under identical excitation and detection conditions. All scale bars

represent 10 μm. (c) Flow cytometry measurements of the intensity distributions of cells labeled via nonspecific binding (N, negative control) and positive specific targeting (P, positive) using Qdots 525 (QN, Qdot negative control; QP, Qdot positive), BODIPY 520 Pdots (520N, BODIPY 520 negative control; 520P, BODIPY 520 positive), BODIPY 590 Pdots (590, 590P), and BODIPY 680 Pdots (680N, 680P). All Qdots and Pdots were conjugated with streptavidin. Reproduced in part from Rong, Y.; Wu, C.; Yu, J.; Zhang, X.; Ye, F.; Zeigler, M.; Gallina, M. E.; Wu, I. C.; Zhang, Y.; Chan, Y.-H.; Sun, W.; Uvdal, K.; Chiu, D. T. *ACS Nano*, **2013**, 7 (1), 376–384. (ref 21). Copyright 2013 American Chemical Society.

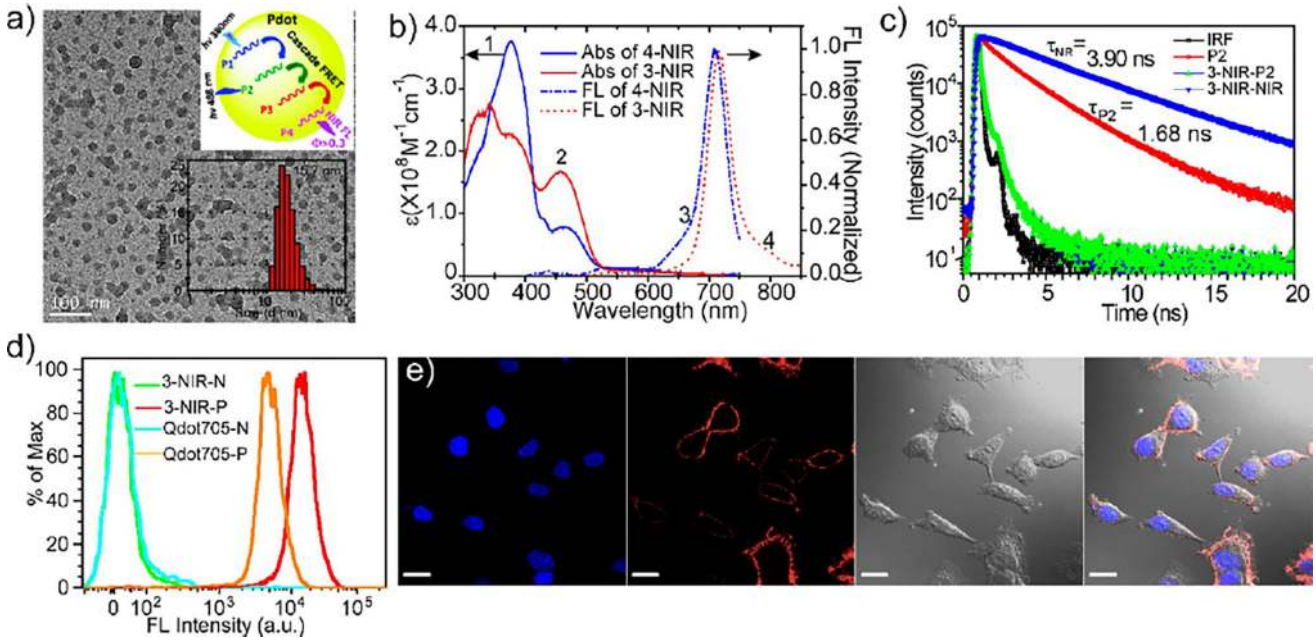

Figure 2.

(a) TEM image of **3-NIR** Pdots (prepared by blending polymers P1, P2, and P4); top inset shows the scheme of the cascade FRET in Pdot; bottom inset is the size distribution measured by DLS. (b) Absorbance (solid line) and fluorescence spectra (dashed line) of **4-NIR** (prepared by blending polymers P1-P4) (blue, λ_{ex} = 380 nm) and **3-NIR** Pdots (red, λ_{ex} = 450 nm). (c) Time-resolved fluorescence decay of polymer **P2** Pdots and **3-NIR** Pdots. (d) Flow-cytometry measurements of the intensity distributions of MCF-7 cells labeled with Qdot705-streptavidin (negative labeling, cyan curve; positive labeling, orange curve) and **3-NIR** Pdot-streptavidin (negative labeling, green curve; positive labeling, red curve). All the positive and negative labeling was completed and measured under identical experimental conditions. In the negative labeling, primary biotinylated antibodies were absent. (e) Confocal fluorescence images of MCF-7 cells positively labeled with **3-NIR** Pdot-streptavidin probes. Images from left to right: blue fluorescence from the nuclear stain Hoechst 34580; deep red fluorescence images from **3-NIR** Pdot-streptavidin probes; Nomarski (DIC) images; combined fluorescence images. Scale bars: 20 μm. Reproduced in part from Zhang, X.; Yu, J.; Rong, Y.; Ye, F.; Chiu, D. T.; Uvdal, K. *Chem. Sci.* **2013**, 4, 2143–2151 (ref 23), with permission of The Royal Society of Chemistry.

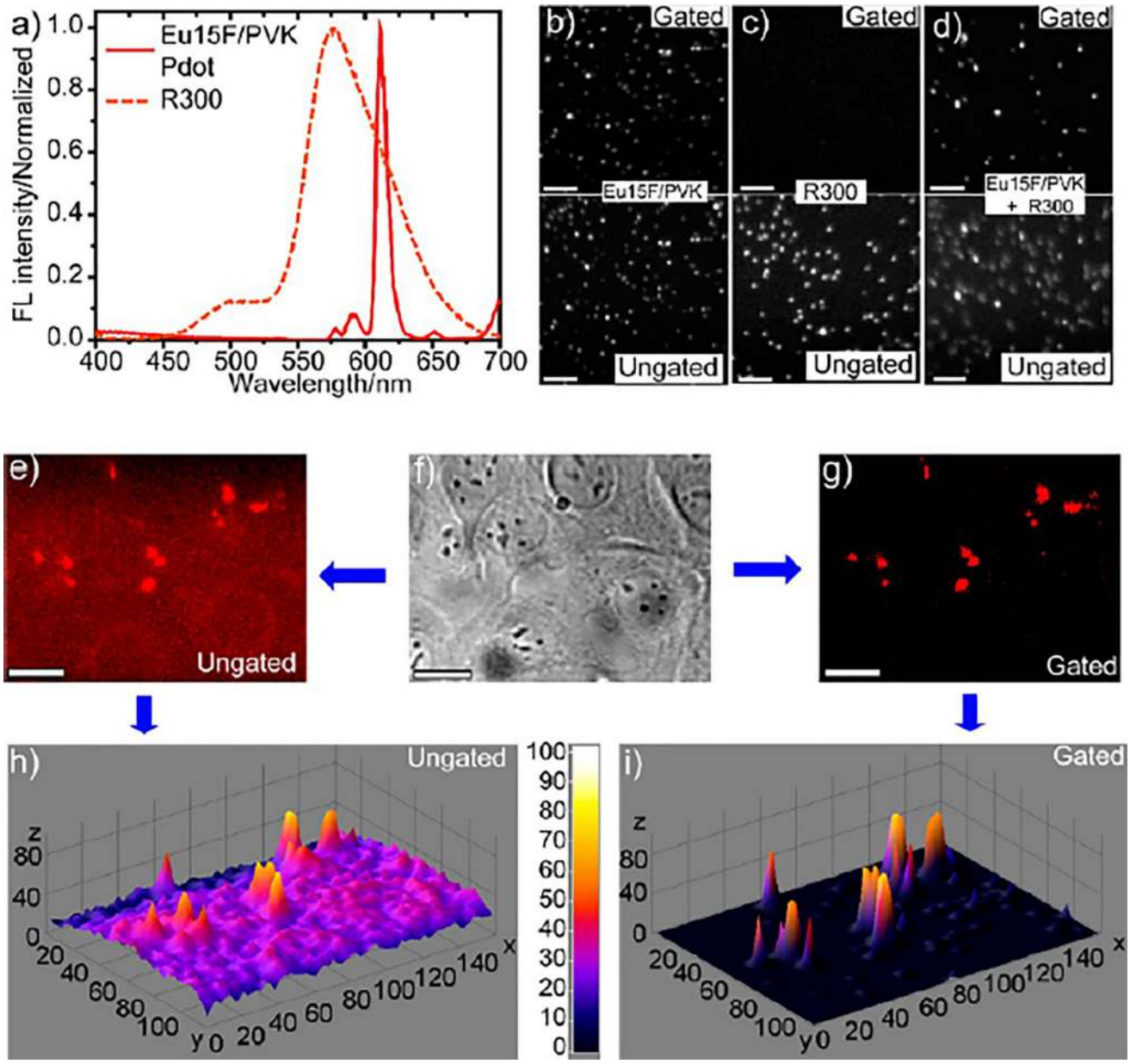

Figure 3.

Eu-complex/PVK Pdots with long luminescence lifetime. (a) Emission spectra of Eu15F/PVK Pdots and 300 nm diameter R300 fluorescent beads (excited at 342 nm). (b–d) Time-gated and ungated single particle images of Eu15F/PVK Pdots, R300 beads, and mixtures of Eu15F/PVK Pdots and R300 beads, respectively: top, gated; bottom, ungated; scale bar represents 5 μm. (e–g) Ungated fluorescence image, bright field image, and time-gated fluorescence image of Eu15F/PVK Pdots in MCF-7 cells; scale bar represents 50 μm. (h) 3D surface plot of ungated image from (e). (i) 3D surface plot of gated image from (g). Reproduced in part from Semiconducting Polymer Dots Doped with Europium Complexes Showing Ultranarrow Emission and Long Luminescence Lifetime for Time-Gated Cellular

Imaging. Sun, W.; Yu, J.; Deng, R.; Rong, Y.; Fujimoto, B.; Wu, C.; Zhang, H.; Chiu, D. T. *Angew. Chem. Int. Ed. Engl.*, Vol. 52, Issue 43 (ref 22). Copyright 2013 Wiley.

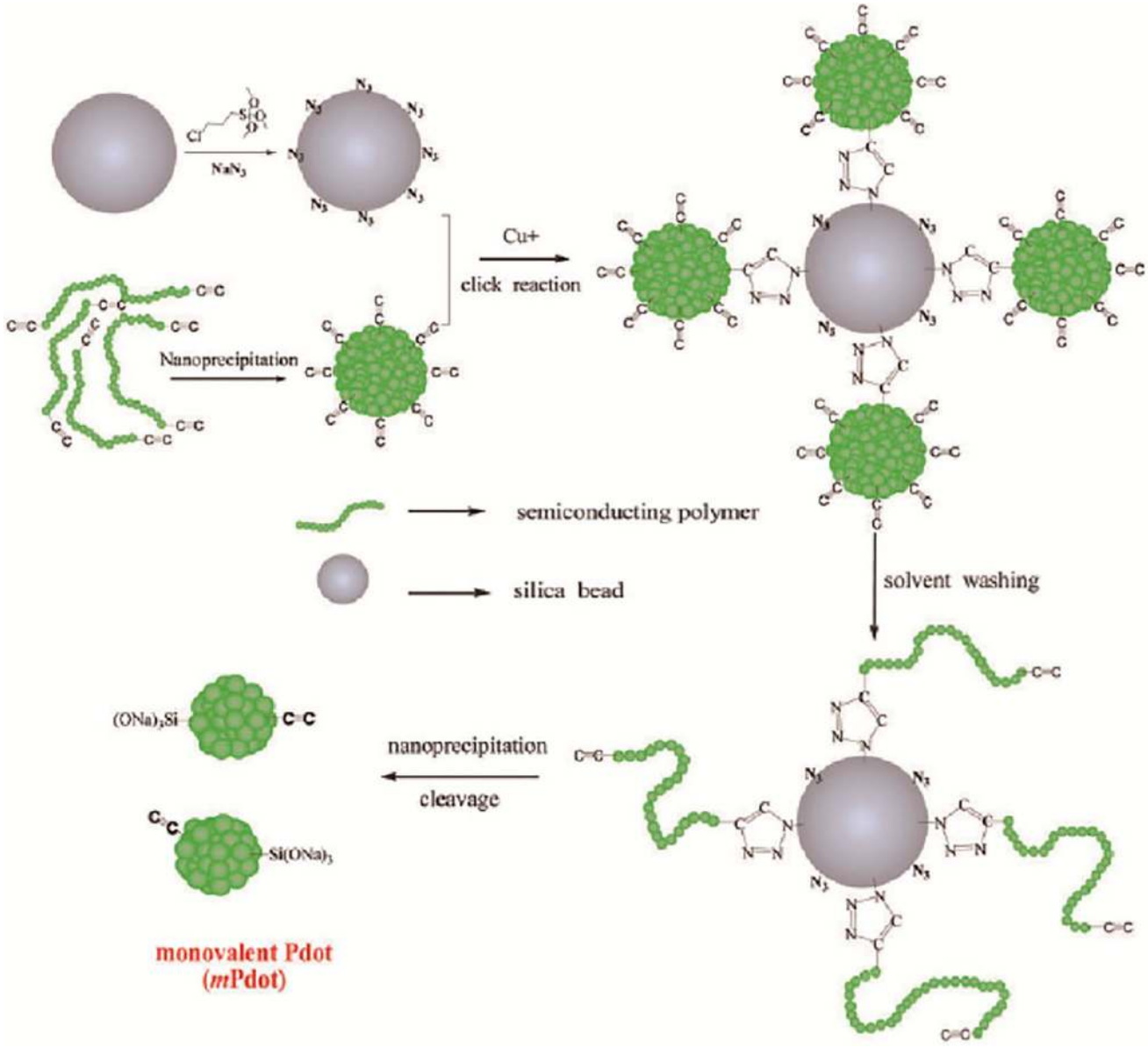

Figure 4.

Procedure to prepare single-chain Pdots (*s*Pdots) and monovalent Pdots (*m*Pdots). A silica particle with a diameter of ~200 nm was prepared and its surface was modified with a layer of chloride (SiO_2–Cl) via the hydrolysis and condensation of chloridetrimethoxysilane. The SiO_2–Cl groups were then modified to azide to form a clickable silica nanoparticle. Separately, regular multivalent PPV–PPA Pdots were prepared using nanoprecipitation; these Pdots had alkyne groups so they could react with SiO_2–N_3 on the silica surface via click chemistry. Once the regular PPV–PPA Pdots were clicked onto the surface of the silica nanoparticle, the solvent was changed from aqueous solution to THF and the silica–polymer complex was washed with THF several times. This step removed all the polymer chains in the regular Pdot that were not covalently attached to the silica surface. The single polymer chains attached to the surface of the silica nanoparticles were then reprecipitated into single-

chain and monovalent *m*Pdots by reintroducing the silica–polymer complex into aqueous solution from THF. Finally, the *m*Pdots were cleaved from the silica surface and released into solution in the presence of NaOH and Triton X-100. To remove NaOH and Triton 100, the *m*Pdot solution was dialyzed overnight in water or buffer. Reproduced from Ye, F.; Wu, C.; Sun, W.; Yu, J.; Zhang, X.; Rong, Y.; Zhang, Y.; Wu, I. C.; Chan, Y.-H.; Chiu, D. T. *Chem. Commun.* **2014**, 50 (42), 5604–5607 (ref 36), with permission of The Royal Society of Chemistry.

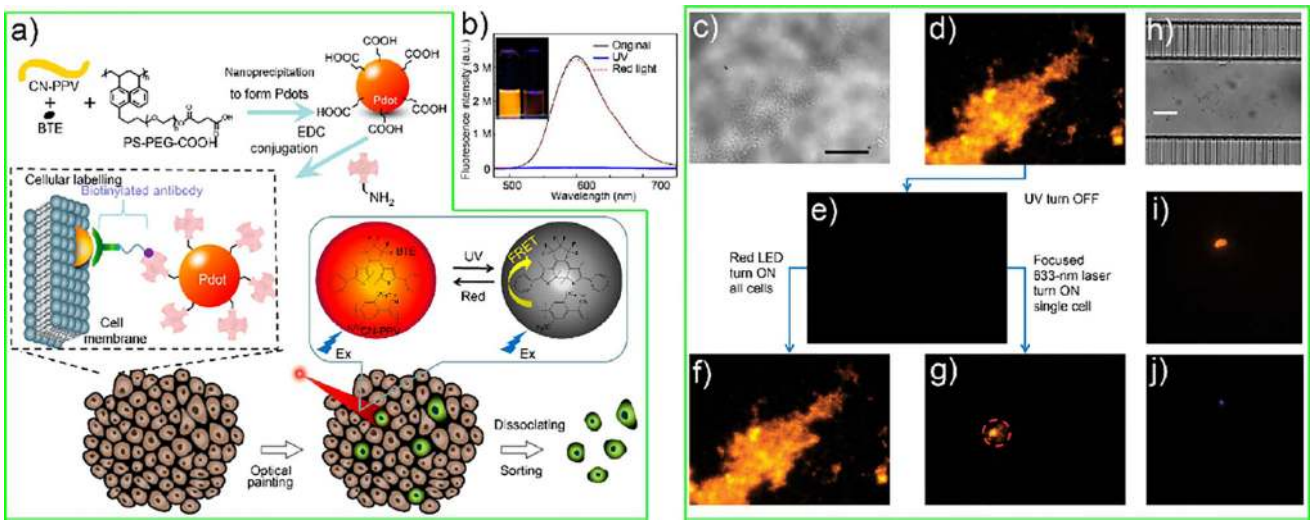

Figure 5.

(a) Schematic depiction of Pdot formation, cellular labeling using Pdots, and optical "painting" of labeled cells with light, followed by the sorting and isolation of the painted cells. (b) The emission spectra (excitation at 450 nm) of the CN-PPV-BTE Pdots in the original ON state (black line), after UV illumination to turn the Pdots into the OFF state (blue line), after red-light illumination to return the Pdots to the ON state (red dashed line). The inset shows the photograph of the Pdot solution in the ON and OFF states. (c, d) A bright-field and fluorescence image of a tissue slice labeled with photoswitchable Pdots. (e) Application of UV light turned "off" the fluorescence of all cells in the tissue. (f, g) Fluorescence images showing the turning "on" of all cells in the tissue with wide-field illumination using a red LED (f), as well as the selective painting and turning "on" of a single cell in the tissue with a focused 633 nm laser beam (g). (h–j) The painted cells could be sorted and recovered and then observed under bright field (h), Pdot fluorescence (i), and DAPI (nuclear stain) fluorescence (j). Scale bar, 20 μm. Adapted from Kuo, C.-T.; Thompson, A. M.; Gallina, M. E.; Ye, F.; Johnson, E. S.; Sun, W.; Zhao, M.; Yu, J.; Wu, I. C.; Fujimoto, B.; DuFort, C. C.; Carlson, M. A.; Hingorani, S. R.; Paguirigan, A. L.; Radich, J. P.; Chiu, D. T., Optical painting and fluorescence activated sorting of single adherent cells labeled with photoswitchable Pdots. *Nat. Commun.* **2016**, 7, 11468. (ref 41), Copyright 2016, Rights Managed by Nature Publishing Group.

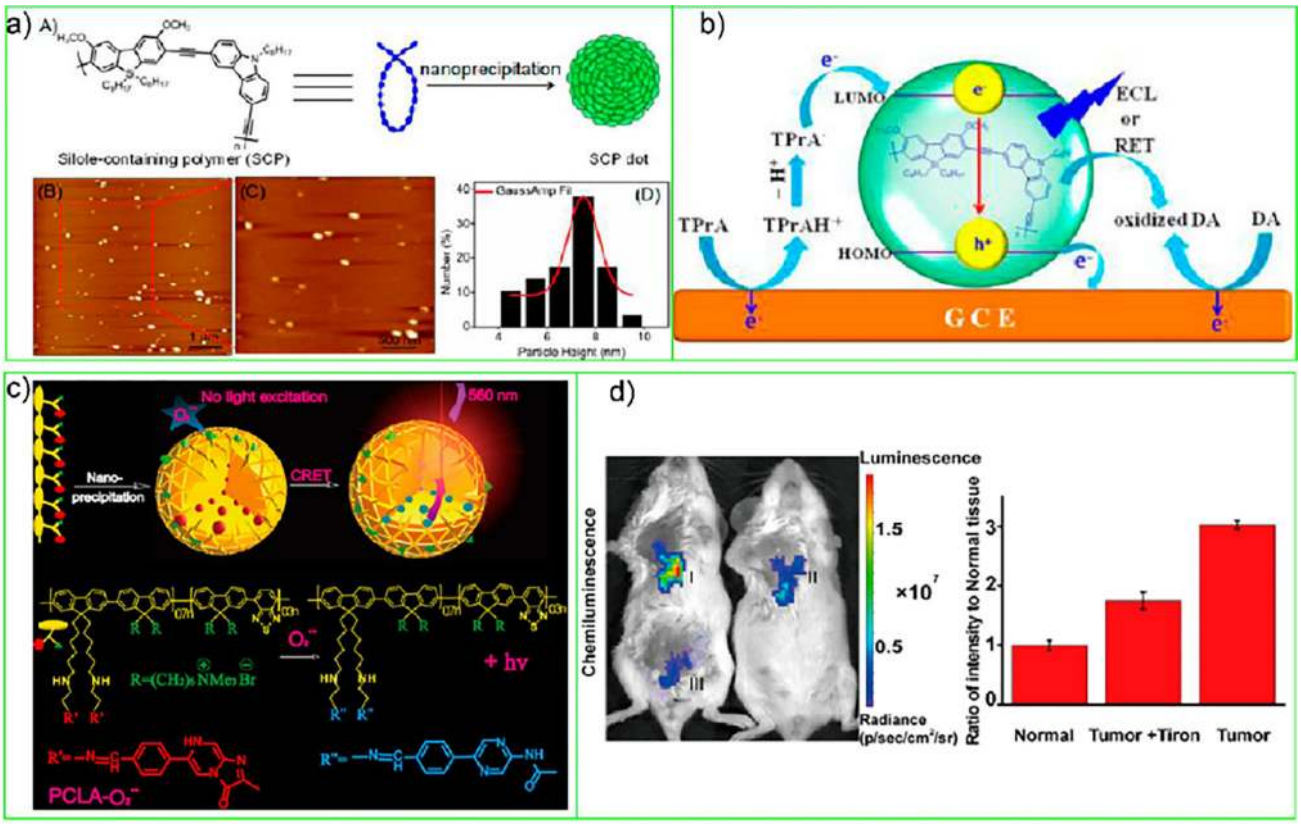

Figure 6.

(a) Scheme of the formation of SCP Pdots and their AFM images. (b) Proposed ECL mechanism of the SCP Pdot/TPrA system and ECL quenching mechanism by dopamine through resonance energy transfer. Reproduced from Feng, Y.; Lei, J.; Ju, H.; Dai, C.; Cheng, Y., *Anal. Chem.* **2016**, 88 (1), 845-50 (ref 50). Copyright 2016 American Chemical Society. (c) Schematic illustration of CL Pdot preparation by nanoprecipitation, $O_2^{\bullet-}$ sensing of PCLA-$O_2^{\bullet-}$, and the structure of PCLA-$O_2^{\bullet-}$. (d) Representative images (pseudocolor) of mice tumor (I), tumor + Tiron (II), and normal (III) tissue followed by PCLA-$O_2^{\bullet-}$ ($n = 3$). Images ($\lambda_{em} = 570 \pm 10$ nm) were acquired using an IVIS Lumina II at 30 s after PCLA-$O_2^{\bullet-}$ administration and quantitative CL intensities of (**I-III**). Reproduced in part from Li, P.; Liu, L.; Xiao, H.; Zhang, W.; Wang, L.; Tang, B., *J. Am. Chem. Soc.* **2016**, 138 (9), 2893–2896 (ref 51). Copyright 2016 American Chemical Society.

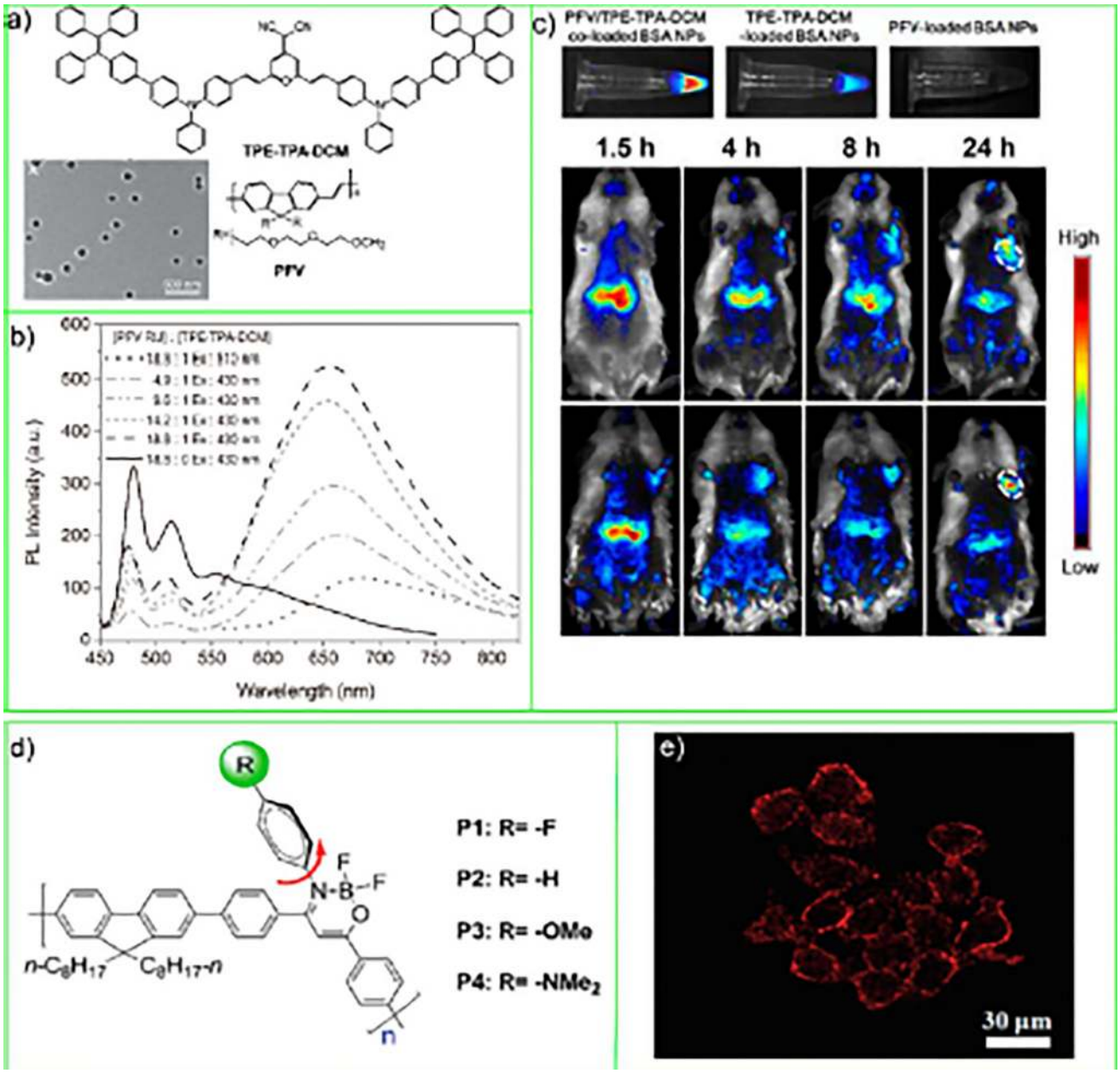

Figure 7.

(a) Chemical structures of PFV host polymer and TPE-TPA-DCM molecules and TEM image of the PFV/TPE-TPA-DCM coloaded BSA CPNs. (b) PL spectra of PFV/TPE-TPA-DCM coloaded BSA CPNs in water. (c) In vitro fluorescence images of aqueous solutions containing PFV/ TPE-TPA-DCM coloaded, TPE-TPA-DCM-loaded, and PFV-loaded BSA CPNs. In vivo fluorescence imaging of tumor-bearing mice after intravenous injection of PFV/TPE-TPA-DCM coloaded BSA CPNs (b) and PFV/TPE-TPA-DCM coloaded BSA-RGD CPNs. The white circles indicate the tumor sites. Reproduced in part from Ding, D.; Li, K.; Qin, W.; Zhan, R.; Hu, Y.; Liu, J.; Tang, B. Z.; Liu, B., Conjugated Polymer Amplified Far-Red/Near-Infrared Fluorescence from Nanoparticles with Aggregation-Induced Emission Characteristics for Targeted In Vivo Imaging. *Adv. Healthcare Mater.*

2013, 2 (3), 500–507 (ref 57). Copyright 2013 Wiley. (d) Chemical structures of conjugated polymers **P1-P4**. (e) Confocal fluorescnece images of HeLa cells stained with **P1** CPNs. Reproduced in part from Dai, C.; Yang, D.; Fu, X.; Chen, Q.; Zhu, C.; Cheng, Y.; Wang, L., *Polym. Chem.* **2015**, 6 (28), 5070–5076 (ref 58), with permission of The Royal Society of Chemistry.

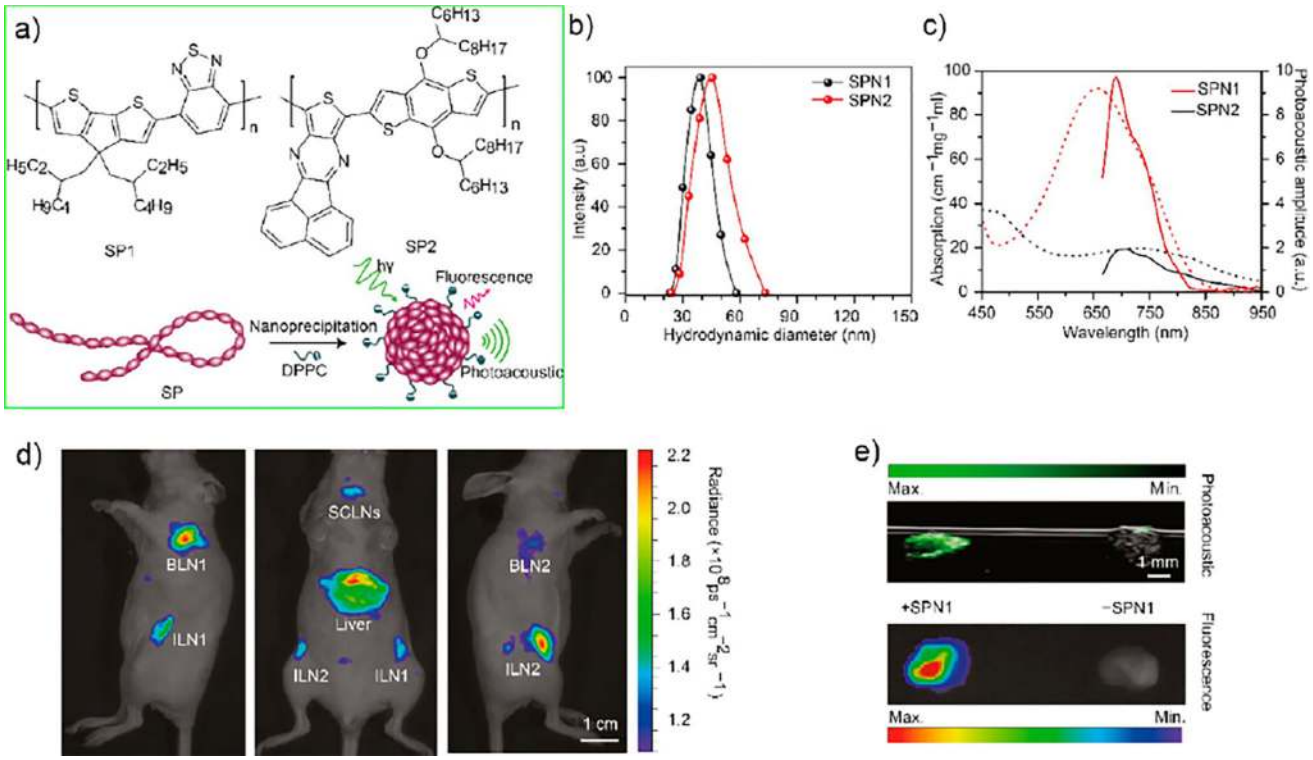

Figure 8.

(a) Molecular structures of semiconducting polymers (SP) SP1 and SP2 used for the preparation of CPNs for fluorescence and photoacoustic imaging. Schematic of the preparation of SP nanoparticles (SPNs) through nanoprecipitation. SP is represented as a long chain of chromophore units (red oval beads). 1,2-Dipalmitoyl-*sn*-glycero-3-phosphocholine (DPPC) is represented by a short hydrophobic tail and a charged head. (b) Representative DLS profiles of SPNs. (c) Ultraviolet–visible absorption (dashed lines) and photoacoustic spectra (solid lines) of SPNs. (d) Fluorescence/bright-field images of the corresponding mouse. (e) Ex vivo photoacoustic/ultrasound coregistered (top) and fluorescent/bright-field (bottom) images of resected lymph nodes from the mouse with SPN1 injection (50mg/mouse) (left) or a control mouse without SPN1 injection (right) in an agar phantom. Reproduced in part from Pu, K.; Shuhendler, A. J.; Jokerst, J. V.; Mei, J.; Gambhir, S. S.; Bao, Z.; Rao, J., Semiconducting polymer nanoparticles as photoacoustic molecular imaging probes in living mice. *Nat. Nanotechnol.* **2014**, 9 (3), 233–239 (ref 63), Copyright 2014, Rights Managed by Nature Publishing Group.

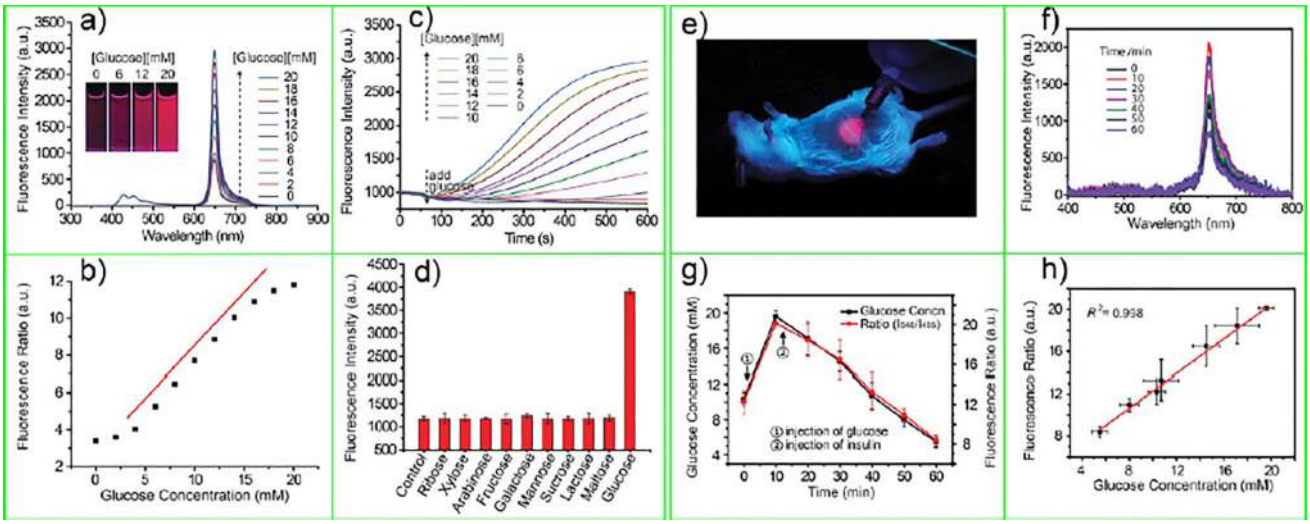

Figure 9.

(a) Emission spectra of the Pdot-GOx sensor at different glucose concentrations; the inset shows aqueous dispersions of Pdot-GOx in the presence of different glucose concentrations under a UV lamp (365 nm). (b) Ratiometric calibration plot (I_{648}/I_{428}) of the Pdot-GOx sensor as a function of glucose concentration. (c) Response curves of the Pdot-GOx to glucose in aqueous suspensions. (d) Selectivity of the Pdot-GOx sensor for glucose over potential interfering carbohydrates. (e) Photograph of a mouse subcutaneously injected with Pdot-GOx under 385 nm light excitation. (f) Evolution of fluorescence emission spectra of the implanted Pdot-GOx sensor in a live mouse with administration of glucose and insulin. (g) Intensity ratio of 650–480 nm emission (red data) obtained from the emission spectra in (b) and the glucose concentrations measured from the tail blood (black data). The blood glucose level was elevated and decreased by sequential intraperitoneal injection of glucose and insulin. (h) Emission intensity ratio as a function of blood glucose concentration. Reproduced from Sun, K.; Tang, Y.; Li, Q.; Yin, S.; Qin, W.; Yu, J.; Chiu, D. T.; Liu, Y.; Yuan, Z.; Zhang, X.; Wu, C., *ACS Nano* **2016**, 10 (7), 6769–6781 (ref 79). Copyright 2016 American Chemical Society.

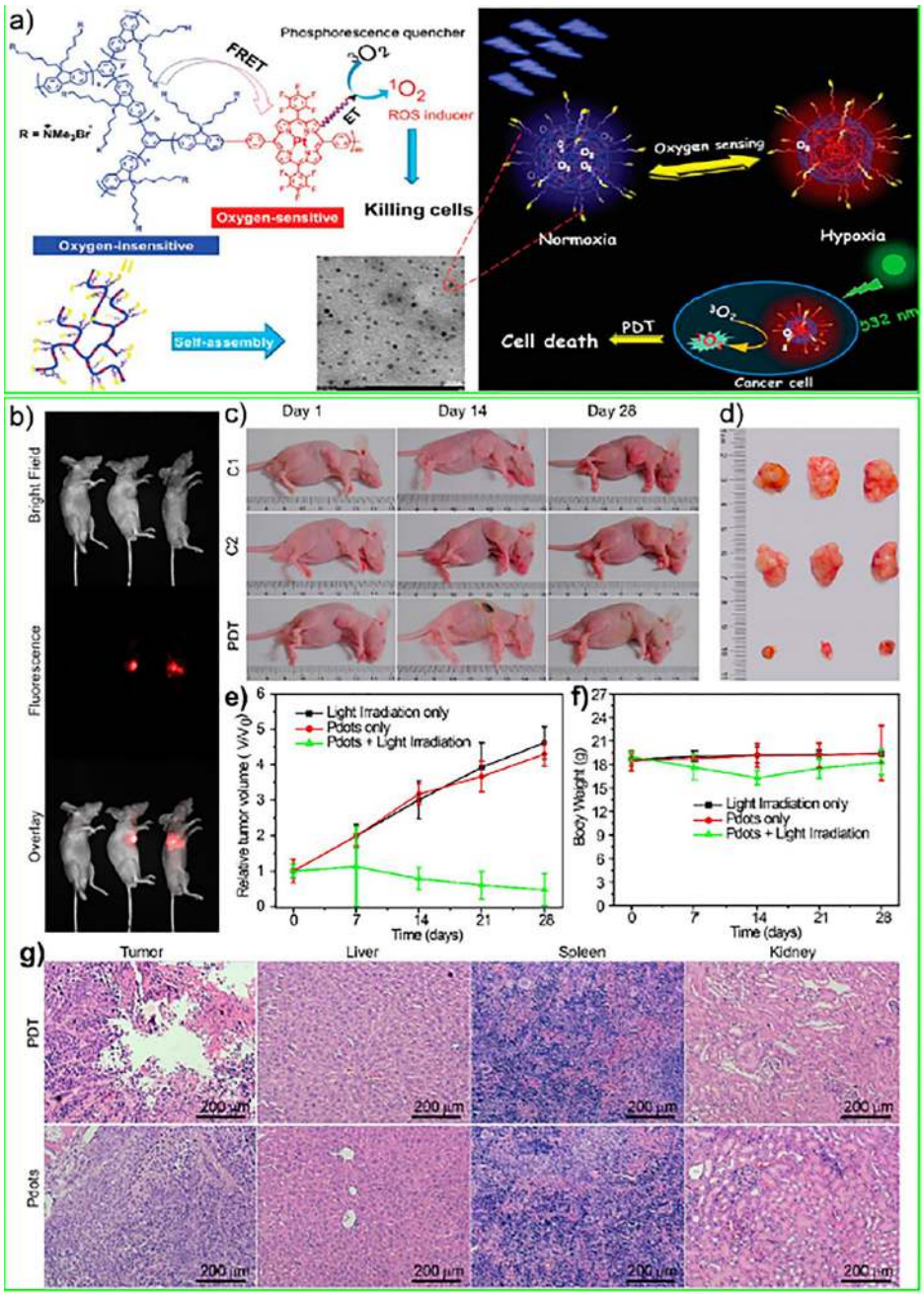

Figure 10.

(a) Chemical structures of conjugated polymer P2, TEM image (Pdots in PBS solution, scale bar = 20 nm), self-assembly, O_2 sensing, and PDT mechanisms of phosphorescent Pdots. Reproduced from Zhou, X.; Liang, H.; Jiang, P.; Zhang, K. Y.; Liu, S.; Yang, T.; Zhao, Q.; Yang, L.; Lv, W.; Yu, Q.; Huang, W., Multifunctional Phosphorescent Conjugated Polymer Dots for Hypoxia Imaging and Photodynamic Therapy of Cancer Cells. *Adv. Sci.* (Weinheim, Ger.) **2016**, 3 (2), 1500155 (ref 86). Copyright 2016 Wiley. In vivo imaging and photodynamic therapy of PFBT-TPP Pdots. (b) Whole-animal imaging of tumor-bearing mice with intratumoral injection of PFBT-TPP Pdots (from top to bottom: bright field,

fluorescence, and overlay). (c) Representative photographs of the tumor-bearing mice after various treatments on the first, 14th, and 28th day. The top panel shows control mice with intratumoral Pdot injection only (C1 group), the middle panel shows mice treated with light irradiation only (C2 group), and the bottom panel shows mice treated with intratumoral Pdot injection and light irradiation (PDT group). (d) Representative photographs of the tumors collected from the mice after various treatments. The tumors collected from the C1 group, C2 group, and PDT group were shown in the upper, middle, and lower rows, respectively. (e) Tumor growth curves in the tumor-bearing mice after different treatments. Tumor volumes were normalized to their initial sizes. Error bars represent the standard deviation of 10 mice per group. (f) Time-dependent body weight changes of the mice after various treatments. (g) Histological H&E staining of various organs from the mice of PDT and control groups. Reproduced from Chang, K.; Tang, Y.; Fang, X.; Yin, S.; Xu, H.; Wu, C., *Biomacromolecules* **2016**, 17 (6), 2128–2136 (ref 83). Copyright 2016 American Chemical Society.